

Advanced therapeutic inhalation aerosols of a Nrf2 activator and RhoA/Rho kinase (ROCK) inhibitor for targeted pulmonary drug delivery in pulmonary hypertension: design, characterization, aerosolization, *in vitro* 2D/3D human lung cell cultures, and *in vivo* efficacy

Maria F. Acosta, Priya Muralidharan, Carissa L. Grijalva, Michael D. Abrahamson, Don Hayes Jr., Jeffrey R. Fineman, Stephen M. Black and Heidi M. Mansour 

Abstract: Inhalable nanostructured microparticles of simvastatin, a Nrf2 activator and RhoA/Rho kinase (ROCK) inhibitor, were rationally designed for targeted pulmonary delivery as dry powder inhalers (DPIs) for the treatment of pulmonary hypertension (PH). Advanced particle engineering design technology was employed to develop inhalable dry powders using different dilute feed concentrations and spray drying pump rates. Several analytical techniques were used comprehensively to characterize the physicochemical properties of the resulting powders. Scanning electron microscopy (SEM) was used to visualize particle morphology (shape), surface structure, size, and size distribution. Karl Fischer titration (KFT) was employed to quantify the residual water content in the powders. X-ray powder diffraction (XRPD) was used to determine crystallinity. Hot-stage microscopy (HSM) under cross-polarizing lens was used to observe the presence or absence of birefringence characteristic of crystallinity. Differential scanning calorimetry (DSC) was employed to quantify thermotropic phase behavior. Attenuated total reflectance (ATR)-Fourier-transform infrared (FTIR) spectroscopy and Raman spectroscopy were used to determine the molecular fingerprint of simvastatin powders before and after particle engineering design. *In vitro* aerosol dispersion performance was performed with three different Food and Drug Administration (FDA)-approved human DPI devices. Cell viability and transepithelial electrical resistance (TEER) were demonstrated using different *in vitro* human pulmonary cell two and three-dimensional models at the air-liquid interface, and *in vivo* safety in healthy rats by inhalation. Efficacy was demonstrated in the *in vivo* lamb model of PH. Four different inhalable powders of simvastatin were successfully produced. They possessed nanostructured surfaces and were in the inhalable size range. Simvastatin retained its crystallinity following particle engineering design. The more dilute feed concentration spray dried at the lower pump rate produced the smallest particles. All powders successfully aerosolized with all three DPI human devices. Inhaled simvastatin as an aerosol restored the endothelial function in the shunt lamb model of PH, as demonstrated by the reduction of pulmonary vascular resistance (PVR) in response to the endothelium-dependent vasodilator acetylcholine.

The reviews of this paper are available via the supplemental material section.

Keywords: advanced spray drying, dry powder inhalers, inhalation aerosol medicine, *in vitro* human cells, *in vivo* lamb, *in vivo* rat, targeted pulmonary drug delivery

Received: 19 January 2021; revised manuscript accepted: 27 January 2021.

Ther Adv Respir Dis

2021, Vol. 15: 1–25

DOI: 10.1177/
1753466621998245

© The Author(s), 2021.

Article reuse guidelines:
sagepub.com/journals-
permissions

Correspondence to:

Heidi M. Mansour
Skaggs Pharmaceutical
Sciences Center, The
University of Arizona
College of Pharmacy,
Tucson, AZ, USA

Department of Medicine,
Division of Translational
and Regenerative
Medicine, The University
of Arizona College of
Medicine, Tucson, AZ, USA

The University of Arizona,
BI05 Institute, Tucson,
AZ, USA

mansour@pharmacy.arizona.edu

Maria F. Acosta
Priya Muralidharan
Michael D. Abrahamson
Skaggs Pharmaceutical
Sciences Center, The
University of Arizona
College of Pharmacy,
Tucson, AZ, USA

Carissa L. Grijalva
Skaggs Pharmaceutical
Sciences Center, The
University of Arizona
College of Pharmacy,
Tucson, AZ, USA

Department of Biomedical
Engineering, The
University of Arizona
College of Engineering,
Tucson, AZ, USA

Don Hayes Jr.
Departments of Pediatrics
and Internal Medicine,
Lung and Heart-Lung
Transplant Programs,
The Ohio State University
College of Medicine,
Columbus, OH, USA

The Davis Heart and Lung
Research Institute, The
Ohio State University
College of Medicine,
Columbus, OH, USA

Jeffrey R. Fineman
Department of Pediatrics,
University of California
San Francisco School of
Medicine, San Francisco,
CA, USA

Stephen M. Black
Department of Medicine,
Division of Translational
and Regenerative
Medicine, The University
of Arizona College of
Medicine, Tucson, AZ, USA
Department of Medicine,
Center for Lung Vascular
Pathobiology, The
University of Arizona
College of Medicine,
Tucson, AZ, USA
Department of Physiology,
The University of Arizona
College of Medicine,
Tucson, AZ, USA

Introduction

Pulmonary hypertension (PH) is a life-threatening disease characterized by an increase in pulmonary arterial pressure^{1–3} and PH occurs in both children⁴ and adults. Other pulmonary diseases such as chronic obstructive pulmonary disease (COPD),⁵ cystic fibrosis (CF),^{6–8} and idiopathic pulmonary fibrosis (IPF)^{9,10} can co-exist with PH. Mitochondrial lung dysfunction and an increase in reactive oxygen species (ROS) production causing oxidative stress have been observed in pulmonary diseases such as PH,¹¹ acute lung injury,¹² and acute respiratory distress syndrome (ARDS).¹² In PH, the overproduction of ROS contributes to pulmonary vascular endothelium damage, pulmonary arterial vasoconstriction, and pulmonary vascular remodeling.¹¹

Simvastatin is a lipophilic statin drug and a 3-hydroxy-3-methyl-3-glutaryl coenzyme A (HMG-CoA) reductase inhibitor used clinically to lower serum cholesterol. However, recent studies have shown that statins have several important pharmacological effects. Statins including simvastatin pharmacologically inhibit the RhoA/Rho kinase (ROCK) pathway^{13–15} and thereby reduce hypertension^{13,15} including pulmonary arterial hypertension^{16–24} in animal models. Simvastatin oral treatment of PH has been reported in patients.²⁵ Cigarette-induced emphysema and PH have been treated successfully with oral simvastatin in rats.²⁶ Radiation-induced lung injury (RILI) has been treated with simvastatin in a mouse-model of RILI.²⁷ In addition to inhibiting the ROCK pathway, simvastatin has the important pharmacological anti-oxidant protective property of being a Nrf2 activator.^{28–31} The Nrf2 pathway plays an important role in lung diseases such as acute lung injury, as we have reported.³²

Pressurized metered-dose inhalers (pMDIs),^{33–35} dry powder inhalers (DPIs),^{36–39} nebulizers,^{40,41} and soft-mist inhalers (SMIs)^{42–44} are used currently in patients for inhalation aerosol therapy for the treatment of many pulmonary diseases. Pulmonary delivery by inhalation aerosols is the clinical gold standard route of administration for pulmonary disease therapies. Simvastatin has been locally delivered by liquid aerosol inhalation to treat respiratory diseases such as asthma in a mouse model⁴⁵ and has been prepared as a DPI prepared by dry jet milling⁴⁶ (which is simply a particle size reduction method but not a particle engineering design technology) but was not tested *in vivo* as a DPI. There are no published reports to the authors'

knowledge of using inhaled simvastatin aerosols to treat PH or any other pulmonary vascular disease.

The objectives of this systematic study were: (1) to use advance particle engineering technology rationally to design simvastatin, a lipophilic drug, as inhalable solid-state particles by advanced organic solution spray drying in closed-mode tailored with the essential properties needed for targeted pulmonary drug delivery as DPIs; (2) comprehensively to characterize the physicochemical properties of simvastatin inhalable powders; (3) comprehensively to characterize *in vitro* aerosol performance using Food and Drug Administration (FDA)-approved human DPI devices with different shear stress device properties; (4) to examine biocompatibility, cell viability, and transepithelial electrical resistance (TEER) *in vitro* on human pulmonary cell two-dimensional (2D) and three-dimensional (3D) models including primary pulmonary cells at the air-liquid interface as a function of simvastatin dose; and (5) to demonstrate the safety and efficacy of inhaled simvastatin aerosols in two different *in vivo* animal models including a healthy rodent model (rat) and a higher animal model in a validated lamb model of PH disease. To the authors' knowledge, this is the first study to report such findings using this approach and these conditions.

Experimental: materials and methods

Materials

Simvastatin (Sim) United States Pharmacopeia (USP) grade [C₂₅H₃₈O₅; molecular weight (MW): 418.566 g/mol] was obtained from ACROS (New Jersey, NJ, USA). Methanol (HPLC-High Pressure Liquid Chromatography-grade, ACS-American Chemical Society-certified grade, purity 99.9%) was obtained from Fisher Scientific (Fair Lawn, NJ, USA). HYDRANAL-Coulomat AD and resazurin sodium salt were from Sigma-Aldrich (St. Louis, MO, USA). Raw and spray dried (SD) Sim powders were stored in sealed glass desiccators over indicating Drierite/Drierite desiccant at –20°C under ambient pressure. Ultra-high purity (UHP) nitrogen gas was acquired from the University of Arizona Cryogenics and Gas facility (Tucson, AZ, USA).

Human pulmonary cell lines A549 [American Type Culture Collection (ATCC) CCL-185], NCI-H358 (ATCC CRL-5807), and Calu-3

(ATCC HTB-55) were purchased from ATCC (Manassas, VA, USA). Dulbecco's modified Eagle's medium (DMEM), advanced 1X, fetal bovine serum (FBS), Pen-Strep, Fungizone, and L-glutamine were obtained from GIBCO by Life Technologies (Thermo Fisher Scientific Inc., Waltham, MA, USA). Eagle's minimum essential medium (EMEM) was obtained from the ATCC as well.

SmallAir is a unique 3D human small airway epithelia comprised of primary cells at the air-liquid interface (ALI) that is reconstituted *in vitro* with its SmallAir special growth media, which is serum-free and contains growth factors plus phenol red. Both were purchased from Epithelix (Geneva, Switzerland).

The 3-week-old male Sprague-Dawley rats (220–270 g) were purchased from Charles River Laboratories International Inc. (Wilmington, MA, USA).

The shunt lamb model of PH was approved by the National Institute of Health (NIH) guidelines for the care and use of laboratory animals. The Committee on Animal Research of the University of California, San Francisco (UCSF) approved all protocols and procedures.

Methods

Preparation of respirable powders by organic solution advanced spray drying (no water) in closed mode. Using conditions similar to those previously reported,^{47,48} advanced organic solution spray drying processing in the absence of water was performed using a Büchi B-290 Mini Spray Dryer with a high performance cyclone in closed-mode using UHP dry nitrogen gas as the atomizing and drying gas and connected to a B-295 Inert Loop (Büchi Labortechnik AG, Flawil, Switzerland). Sim was spray dried under: (a) feed concentration (FC) (0.1% w/v and 0.5% w/v in methanol); and (b) pump rate (PR) (25%, 50%, 75% and 100%). The feed solutions were prepared by dissolving the components in methanol using a Branson 7500 ultrasonicator to assist the dissolution. Table 1 lists the spray drying parameters and Table 2 lists the outlet temperatures. The SD particles were separated from the nitrogen drying gas in the high-performance cyclone and collected in a small sample collector. All SD powders were carefully stored in sealed scintillation glass vials and stored in sealed desiccators over indicating Drierite/Drierite desiccant at -20°C .

Table 1. Spray drying parameters for particle engineering design.

| Spray drying parameter | Value |
|-----------------------------|------------------------------------------------------------------------------|
| Inlet temperature | 150°C |
| Aspirator rate | 100% (40 m ³ /hour) |
| Pump rate | 25% (7.5 mL/min) 50% (15 mL/min) 75% (22.5 mL/min) 100% (30 mL/min) |
| Gas flow | 670 L/hour (55 mmHg) |
| Feed solution concentration | 0.1% w/v 0.5% w/v |
| Solvent | Methanol |
| Atomizer and drying gas | UHP nitrogen |
| Nozzle type and diameter | Stainless steel (0.7 mm) |
| UHP; ultra-high purity. | |

Table 2. Spraying drying pump rates and feed solution concentrations with corresponding outlet temperatures.

| System composition | Outlet T (°C) |
|---------------------------------------------------|---------------|
| Raw Sim | N/A |
| 0.1% w/v SD Sim (25% PR) | 80 |
| 0.1% w/v SD Sim (50% PR) | 67 |
| 0.5% w/v SD Sim (25% PR) | 86–89 |
| 0.5% w/v SD Sim (50% PR) | 71–72 |
| PR, pump rate; SD, spray dried; Sim, simvastatin. | |

Scanning electron microscopy. Using conditions similar to previously reported^{47,49} visual imaging and analysis of particle size, particle morphology (shape), and surface structure were achieved by scanning electron microscopy (SEM) using a FEI Inspect S microscope (FEI, Brno, Czech Republic). Samples were placed on double-sided adhesive carbon tabs (TedPella, Inc., Redding, CA, USA), which were adhered to aluminum stubs (TedPella, Inc.) and were coated with a gold thin film using a Hummer 6.2 sputtering system from Anatech (Union City, CA, USA). The coating process was operated at 15AC milliAmperes with about 7kV of voltage for 90s. The electron beam with an accelerating voltage of 30kV was used at a working distance of 9–12.5 mm. Several magnification levels were used.

Particle sizing and size distribution image analysis using SEM micrographs. The mean size, standard deviation, and size range were determined using SigmaScan Pro 5.0.0 (SYSTAT Software, Inc., San Jose, CA, USA) based on their scanning electron micrographs using a similar procedure that we have previously reported.^{49,50} Representative micrographs for each SD powder at 3000× magnification were analyzed by measuring the diameter of at least 100 particles per sample which is the same number of particles as previously reported.^{48–51}

X-Ray powder diffraction. Using conditions similar to those previously reported,^{47,49} the degree of long-range molecular order (crystallinity) of all powders was measured by X-ray powder diffraction (XRPD). XRPD patterns of samples were collected at room temperature with a PANalytical X'pert diffractometer (PANalytical Inc., Westborough, MA, USA) equipped with a programmable incident beam slit and an X'Celerator Detector. The X-ray radiation used was Ni-filtered Cu K α (45 kV, 40 Ma, and $\lambda = 1.5418 \text{ \AA}$). Measurements were taken between 5.0° and 60.0° (2 θ) with a scan rate of 2°/min. The powder samples were loaded on zero background silicon sample holder.

Differential scanning calorimetry. Using conditions similar to those previously reported,^{47,49} thermal analysis and phase transition measurements were performed on a TA Q1000 differential scanning calorimeter (DSC) (TA Instruments, New Castle, DE, USA) equipped with T-Zero technology, a RSC90 automated cooling system, and an auto sampler. The instrument was previously calibrated with indium. Approximately 1–5 mg of powder was placed into an anodized aluminum hermetic DSC pan. The T-Zero DSC pans were hermetically sealed with the T-Zero hermetic press (TA Instruments). For all the experiments, an empty hermetically sealed aluminum pan was used as reference. UHP nitrogen was used as the purging gas at a rate of 40 mL/min. The samples were heated from at least 0.00°C to 200.00°C at a scanning rate of 5.00°C/min. All measurements were carried out in triplicate ($n = 3$).

Hot-stage microscopy under cross-polarizers. Hot-stage microscopy (HSM) was performed using a Leica DMLP cross-polarized microscope (Wetzlar, Germany) equipped with a Mettler FP 80 central processor heating unit and Mettler FP82 hot stage (Columbus, OH, USA). Using

similar conditions as previously reported,^{47,49} samples were fixed on a glass slide and heated from 25.0°C to 200.0°C at a heating rate of 5.00°C/min. The images were digitally captured using a Nikon Coolpix 8800 digital camera (Nikon, Tokyo, Japan) under 10× optical objective and 10× digital zoom.

Karl Fischer titration. Using conditions similar to those previously reported,^{47,49} the residual water content of all powders was quantified analytically by coulometric Karl Fischer titration (KFT) using a TitroLine 7500 trace titrator (SI Analytics, Weilheim, Germany) following similar conditions reported in other studies. Approximately 1–5 mg of powder was added to the titration cell containing Hydranal Coulomat AD reagent.

Raman spectroscopy. Using similar conditions to those previously reported,⁴⁹ Raman⁵² spectra were obtained at 514 nm laser excitation using a Renishaw InVia Reflex (Gloucestershire, UK) at the surface using a 20× magnification objective on a Leica DM2700 optical microscope (Wetzlar, Germany). This Renishaw system has a 2400 l/mm grating, with a slit width of 65 μm and a thermoelectrically cooled Master Renishaw CCD detector. The laser power was adjusted to achieve 5000 counts per second for the 520 cm^{-1} line of the internal Si Reference. Raman spectra were achieved using 1% of laser power, and 10 seconds of exposure in all samples.

Attenuated total reflectance-Fourier-transform infrared spectroscopy. A Nicolet Avatar 360 Fourier-transform infrared (FTIR) spectrometer (Varian Inc., CA, USA) equipped with a DTGS detector and a Harrick MNP-Pro (Pleasantville, NY, USA) attenuated total reflectance (ATR) accessory was used for this kind of spectroscopy. Each spectrum was collected for 32 scans at a spectral resolution of 2 cm^{-1} over the wavenumber range of 4000–400 cm^{-1} . A background spectrum was carried out under the same experimental conditions. Spectral data were acquired with EZ-OMNIC software. These conditions are similar to those in previous reports.^{47,49}

In vitro aerosol dispersion performance. According to USP Chapter <601> specifications on aerosols,⁵³ the aerosol dispersion performance of SD Sim formulations were tested using the next generation impactor (NGI) (MSP Corporation, Shoreview, MN, USA) with a stainless steel

induction port (USP throat) attachment (NGI model 170; MSP Corporation) equipped with specialized stainless steel NGI gravimetric insert cups (MSP Corporation). Three different FDA-approved human DPI unit-dose capsule-based devices an airflow rate (Q) of 60 L/min were used which were the HandiHaler (Boehringer Ingelheim, Ingelheim, Germany), the NeoHaler (Novartis AG, Stein, Switzerland), and the AeroLizer (Novartis Pharma AG, Basel, Switzerland) which varied in shear stress from highest to medium to lowest, respectively. Using similar conditions described previously,^{47,49} Q was adjusted and measured before each experiment using a Copley DFM 2000 digital flow meter (Copley Scientific, Nottingham, UK). The NGI was connected to a Copley HCP5 high capacity vacuum pump (Copley Scientific, Nottingham, UK) with a Copley TPK 2000 critical flow controller (Copley Scientific, Nottingham, UK).

For the NGI, Q = 60 L/min, the D_{a50} aerodynamic cut-off diameter for each NGI stage was calibrated by the manufacturer and stated as: stage 1 (8.06 μm); stage 2 (4.46 μm); stage 3 (2.82 μm); stage 4 (1.66 μm); stage 5 (0.94 μm); stage 6 (0.55 μm); and stage 7 (0.34 μm). For each NGI stage, powder deposition was quantified gravimetrically with A/E 55 mm diameter glass fiber filters (PALL Corporation, Port Washington, NY, USA) and 75 mm diameter glass fiber filter (Advantec, Japan) for stage 1. Inhalation grade capsules were used and were clear hydroxypropylmethylcellulose (HPMC) size 3 (Qual V, Qualicaps, NC, USA). Each inhalation capsule contained ~10 mg of powder. Three inhalation capsules were used in each experiment. Under ambient conditions, *in vitro* aerosolization was evaluated in triplicate ($n = 3$).

Several aerosol dispersion parameters were determined. The emitted dose (ED) was determined as the difference between the initial mass of powder loaded in the capsules and the remaining mass of powder in the capsules following the aerosolization. The ED (%) in Equation 1 was used to express the percentage of ED based on the total dose (TD) used. The fine particle dose (FPD) was defined as the dose deposited on NGI stages 2–7. The fine particle fraction (FPF %) in Equation 2 was expressed as the percentage of FPD to ED. The respirable fraction (RF %) in Equation 3 was used as the percentage of FPD to total deposited dose (DD) on all NGI stages.

$$\text{Emitted dose fraction (ED\%)} = \frac{\text{ED}}{\text{TD}} \times 100\% \quad (1)$$

$$\text{Fine particle fraction (FPF\%)} = \frac{\text{FPD}}{\text{ED}} \times 100\% \quad (2)$$

$$\text{Respirable fraction (RF\%)} = \frac{\text{FPD}}{\text{DD}} \times 100\% \quad (3)$$

The mass median aerodynamic diameter (MMAD) of aerosol particles and geometric standard deviation (GSD) were calculated using a Mathematica (Wolfram Research, Inc., Champaign, IL, USA) program written by Dr. Warren Finlay.

In vitro 2D human cell culture. The drug dose effect on cell viability was analyzed at different drug concentrations using similar conditions previously reported.^{50,54} The A549 pulmonary cell line is a human alveolar epithelial lung cell line and is also used as a model of the alveolar type I pneumocyte.^{55–57} The H358 pulmonary cell line is a human bronchioalveolar epithelial cell line similar to alveolar type II cells and expresses lung surfactant associated protein A (SP-A).^{55,56} These cell lines were grown in a growth medium including DMEM, advanced 1 \times , 10% (v/v) FBS, Pen-Strep (100 U/mL penicillin, 100 $\mu\text{g/mL}$), Fungizone (0.5 $\mu\text{g/mL}$ amphotericin B, 0.41 $\mu\text{g/mL}$ sodium deoxycholate), and 2 mM L-glutamine in a humidified incubator at 37°C and 5% carbon dioxide (CO_2).

After confluence, A549 and H358, cells were seeded in 96 black well plates at a concentration of 5000 cells/well and 100 μL /well. They were incubated for 48 h to allow attachment to the surface of the plates. Cells were then exposed to different concentrations of the Raw and SD formulations. The drug solutions were prepared by dissolving the powders in 10% ethanol and 90% of non-supplemented DMEM media. A volume of 100 μL of the different drug solution concentrations or control solution (10% ethanol and 90% advanced DMEM) were added to each well. Seventy-two hours after exposure under incubation at 37°C and 5% CO_2 , 20 μL of 20 μM resazurin sodium salt was added to each well and incubated for 4 h. At this point, the fluorescence intensity of the resorufin (metabolite) produced by only viable cells was detected

at 544 nm (excitation) and 590 nm (emission) as previously reported, using the Synergy H1 Multi-Mode Reader (BioTek Instruments, Inc., Winooski, VT, USA). The relative viability of the cell lines was calculated as follow by Equation (4):

$$\text{Relative viability (\%)} = \frac{\text{Sample fluorescence intensity}}{\text{Control fluorescence intensity}} \times 100\% \quad (4)$$

The statistical method used to compare the relative viability between the treated *versus* the non-treated cells was analysis of variance (ANOVA) using SigmaPlot 13 (SYSTAT Software, Inc., San Jose, CA, USA).

In vitro TEER at the ALI on particle exposure to lung epithelial cells. Calu-3, a human lung epithelial cell line derived from bronchial submucosal airway region, was used as a model for monolayer integrity in the upper airways and is known to form tight junctions. Using previously reported similar conditions,^{50,54} cells were grown in a growth medium including EMEM, 10% (v/v) FBS, Pen-Strep (100 U/mL penicillin, 100 µg/mL), Fungizone (0.5 µg/mL amphotericin B, 0.41 µg/mL sodium deoxycholate) in a humidified incubator at 37°C and 5% CO₂. After confluence, the cells were seeded at a concentration of 500,000 cells/mL in Costar (Costar 3460, Corning, NY, USA) Trans-well inserts (0.4 µm polyester membrane, 12 mm for a 12-well plate) from Fisher Scientific (Hampton, NH, USA) with 0.5 mL of media on the apical side and 1.5 mL of media on the basolateral side. Media was changed every other day from the basolateral side. After approximately 1 week of growth, when the cells looked packed and a complete monolayer was visible under the microscope, transepithelial electrical resistance (TEER) values were measured using an EndOhm 12 mm Culture Cup (World Precision Instruments, Sarasota, FL, USA). TEER values of 1000 Ω.cm², were an indicator of a confluent monolayer at liquid-covered culture (LCC). At this point, the media was removed from the apical side in order to facilitate air-liquid interface (ALI) conditions. The TEER responses of the cells were also measured with an EndOhm 12 mm Culture Cup (World Precision Instruments, Sarasota, FL, USA). For TEER measurements at ALL, 0.5 mL of media was added to the apical side of the each Transwell

insert 30 min before the measurement and then immediately removed to return the cells to ALI conditions. After the TEER values reached 500 Ω.cm² (indicating a confluent monolayer at ALI conditions), the cells were exposed to 100 µM of representative SD formulations dissolved in 90:10 media:ethanol to facilitate dissolution. The liquid aerosol formulations were delivered to the Calu-3 cells at ALI using a Penn-Century Micro-Sprayer Aerosolizer model IA-1B (Penn-Century, Inc., Wyndmoor, PA, USA).^{50,55} TEER values were then recorded after 3 h of exposure and then recorded every 24 h up to 7 days after drug exposure using an EndOhm 12 mm Culture Cup (World Precision Instruments, Sarasota, FL, USA), as previously reported.^{50,54}

The statistical method used to compare the TEER values between the treated *versus* the non-treated cells was ANOVA using SigmaPlot 13 (SYSTAT Software, Inc., San Jose, CA, USA).

In vitro cell dose response assay in 3D cell culture at the ALI. The 3D small airway epithelia (Small-Air, Epithelix, Geneva, Switzerland) reconstituted *in vitro* using primary small airways human cells were fully differentiated and functional. The cells were received in 24-well Transwell inserts in a gel matrix. Once the cells were received, they were transferred into a new 24-well plate with 700 µL of the SmallAir media in the basal surface. Media was changed every other day.

After 3 days of incubation at 37°C and 5% CO₂, experiments were performed. For the *in vitro* cell dose response, the cells were exposed to different concentrations of the drug formulation dissolved in 90:10 media:ethanol to facilitate dissolution. After 72 h of incubation, the inserts were rinsed with a 6 µM Resazurin solution in order to eliminate the remaining red phenol from the cell growth media. The inserts were transferred to a new 24-well plate filled with 500 µL/well of Resazurin solution and then 200 µL/well was added in the apical surface. After 1 h of incubation, 100 µL from the apical side was transferred to a 96 black well plate. At this point, the fluorescence intensity of the resorufin (fluorescent metabolite) produced by viable cells was detected at 544 nm (excitation) and 590 nm (emission) using the Synergy H1 Multi-Mode Reader (BioTek Instruments, Inc., Winooski, VT, USA). The relative viability of the cell line was calculated with Equation 4. This protocol was provided by the vendor.⁵⁸

In vitro TEER analysis upon particle exposure to 3D human small airway epithelia at the ALI. As described above, after receiving the cells, they were transferred into a new 24-well plate pre-filled with 700 μ L of SmallAir media on the basal side. After 3 days of incubation the experiments were performed. Cells were exposed to a different concentration of drug solution (1000 μ M, 100 μ M and 50 μ M). TEER values were measured using EVOMX (Epithelial VoltOhmMeter) and electrode (STX2) (World Precision Instruments, Sarasota, FL, USA). To measure TEER, 200 μ L of the cell media was added to the apical surface of the inserts. The long part of the electrode was inserted through the gap of the insert and leaned on the bottom of the well, and the short stem was above in the apical surface, inside the culture media. TEER values were obtained before exposure to the drug solution and after exposure to them. The response was measured after 3 h of exposure and then every 24 h for 5 days. Every time the TEER measurement was finished, the media was removed from the apical surface in order to leave the cells in ALI conditions. This was followed by the protocol given by the vendor.⁵⁸

In vivo healthy rat study. Fifteen male Sprague–Dawley rats with a body weight of 220–270 g and 3 weeks of age were purchased from Charles River Laboratories International, Inc. (Wilmington, MA, USA), for this study. Rats were housed in the University of Arizona animal care (UAC) facility for at least 1 week before being used in the experiments. Animals were kept in a 12-hour light/dark cycle at an ambient temperature of 22°C and received standard rodent food and water ad libitum. All experimental procedures were approved by the Institutional Animal Care and Use Committee at the University of Arizona (IACUC). The local delivery of the aerosols was done non-invasively without any incision into the animal using the Penn-Century Dry Powder Insufflator model DP-4R (Penn-Century Inc., Wyndmoor, PA, USA), which is customized to the respiratory tract of the rat. Three groups with five rats per group were defined for the study which were the following: (a) control (air); (b) SD Sim 25% PR; and (c) SD Sim 50% PR. A single dose of 10 mg/kg of SD Sim 25% PR and SD Sim 50% PR formulations was administered under local short-acting anesthesia using 1–5% isoflurane diluted in air or oxygen. The rodent insufflator atomizer

was placed on the tongue of the animal and slowly fed down into the larynx/trachea region located at the front of the esophagus/neck area to just above the first bifurcation of the bronchi. A small-animal rodent laryngoscope (Penn-Century Inc., Wyndmoor, PA, USA) was used directly to visualize the trachea of the rats. The particles were gently puffed into the lungs of the animals using the small-animal air pump (Penn-Century Inc., Wyndmoor, PA, USA) and the atomizer portion of the insufflator was gently removed from the throat of the animal. Total aerosol treatment took approximately 5–7 min per rat. Rats were closely monitored after recovery to be sure they have no difficulty with respiration, even though this was not expected.

After 3 days, animals were euthanized by an anesthetic cocktail overdose of 100 mg/kg ketamine/10 mg/kg xylazine by intraperitoneal injection which was followed by thoracic incision to remove the lungs, collect terminal blood, and bronchoalveolar lavage fluid (BALF) by three times flushing with isotonic saline. The lungs and respiratory tree were removed and fixed for histopathology.

Enzyme-linked immunosorbent assay. The frozen BALF was thawed on ice and centrifuged at 2000g for 60 min at 4°C. The concentrations of interleukin (IL)-6 and tumor necrosis factor (TNF)- α in the BALF supernatants were measured by sandwich enzyme-linked immunosorbent assay (ELISA) using pair-matched antibodies according to the manufacturer's instructions. The ELISA kits were obtained from eBioscience, Inc. (San Diego, CA, USA) and R&D (Minneapolis, MN, USA).⁴⁵

The statistical method used to compare the concentrations of IL-6 and TNF- α in the BALF supernatants of the treated *versus* the non-treated rats was ANOVA using SigmaPlot 13 software (SYSTAT Software, Inc., San Jose, CA, USA). Three repeats (i.e. triplicates) of the ELISA for each rat were done.

Tissue processing and histological analysis. Whole lungs were taken from rats under terminal anesthesia, as described in the previous section. The whole lungs were inflated with 10% of formalin and immersed in the same solution. The intact whole lungs in formalin were sent in 15 mL centrifuge tubes sealed with parafilm at room

temperature to HistoWiz, Inc. (Brooklyn, NY, USA), an expert professional histology service vendor, where the intact whole lungs were paraffin-embedded, sectioned horizontally into 5 μm slices, and hematoxylin and eosin (H&E) stained using their standard procedure.

In vivo efficacy in the shunt lamb model of PH. A lamb model of PH associated with increased pulmonary blood flow and pressure (PBF) was created, as described.^{59,60} At 4 weeks of age, a shunt lamb was anesthetized and dosed with SD Sim (25% PR) as aerosol in a dose of 6.5 mg/kg. Endothelial function was demonstrated by measuring the pulmonary vascular resistance (PVR) in response to acetylcholine (Ach). The Penn-Century Microsprayer Aerosolizer (Penn Century, Inc., Wyndmoor, PA, USA) was used to deliver simvastatin. The lamb study was performed at UCSF under an approved animal safety protocol.

Statistical analysis. Design of experiments was conducted using Design-Expert 8.0.7.1 software (Stat-Ease Corporation, Minneapolis, MN, USA). A multi-factorial design for SD Sim was utilized for *in vitro* aerosol testing. Interaction of process parameters and the different devices were evaluated using the ANOVA test performed using Design-Expert software. The different interactions on the performance of the formulations were evaluated using the 3D surface plots generated from Design Expert. All experiments were performed at least in triplicate ($n=3$). Results are expressed as mean \pm standard deviation.

Results

Four different systems were developed by spray drying Sim at different conditions of two feed concentrations and two spray drying pump rates. Particles were successfully formed at 0.1% w/v Sim feed concentration at both pump rates of 25% and 50% and at 0.5% w/v Sim feed concentration also at the same two pump rates of 25% PR and 50% PR. It is important to note that other pump rates were tested; however, there was no particle formation.

Scanning electron microscopy

Size and morphology of Raw and SD particles were visualized by SEM. Different magnifications are shown in Figure 1. The particles had equivalent sphere morphology. The surface

morphology was wrinkled, corrugated, and nanoaggregates were observed. Although the particles were formed, they looked agglomerated and sintered. Overall, SEM micrographs showed that particle formation was better at lower FC (0.1% w/v) particularly at 25% PR (Figure 3b). Nevertheless, all SD powders show comparable characteristics.

Particle sizing and size distribution by image analysis of SEM micrographs

As shown in Table 3, all SD powders of Sim had a broad particle size distribution. The geometric mean diameter of the four powders varied and ranged between 6.59 μm and 12.64 μm . It was clear that the geometric mean diameter was smaller for the powders produced at the more dilute feed concentration solution of 0.1% w/v and bigger particles were produced at 0.5% w/v feed concentration solution. This was in good agreement with the SEM micrographs. The higher feed concentration solution produced solid state particles with a larger geometric mean diameter and also the particle size distribution was broader. The low FC powders had a particle size range $\leq 10 \mu\text{m}$, which is preferred for inhalation therapy. Particles were sized at 3000 \times magnification.

X-ray powder diffraction

The XRPD diffraction pattern of raw Sim showed sharp and intense peaks (i.e. long-range molecular order) due to the crystallinity of the drug. Numerous distinctive peaks at a diffraction angle of 2θ (9.10, 16.92, 17.38, 18.47, 19.06, and 22.21) were observed. This was shown in Figure 2, similarly to what has previously been reported.^{61–63} All SD Sim powders showed the same pattern as raw Sim.

Differential scanning calorimetry

The thermograms of the raw and the SD particles are shown in Figure 3. All thermograms were very similar. They presented a small exotherm before the major endotherm. The small exotherm was at around 120°C, whereas the major endotherm was observed at about 130°C. Fast DSC heating scans were conducted at 20°C/min and 40°C/min on all raw and SD Sim powders to detect a possible glass transition temperature (T_g), but no T_g was detected (data not shown). Phase transition temperatures and enthalpies for all systems are summarized in Table 4.

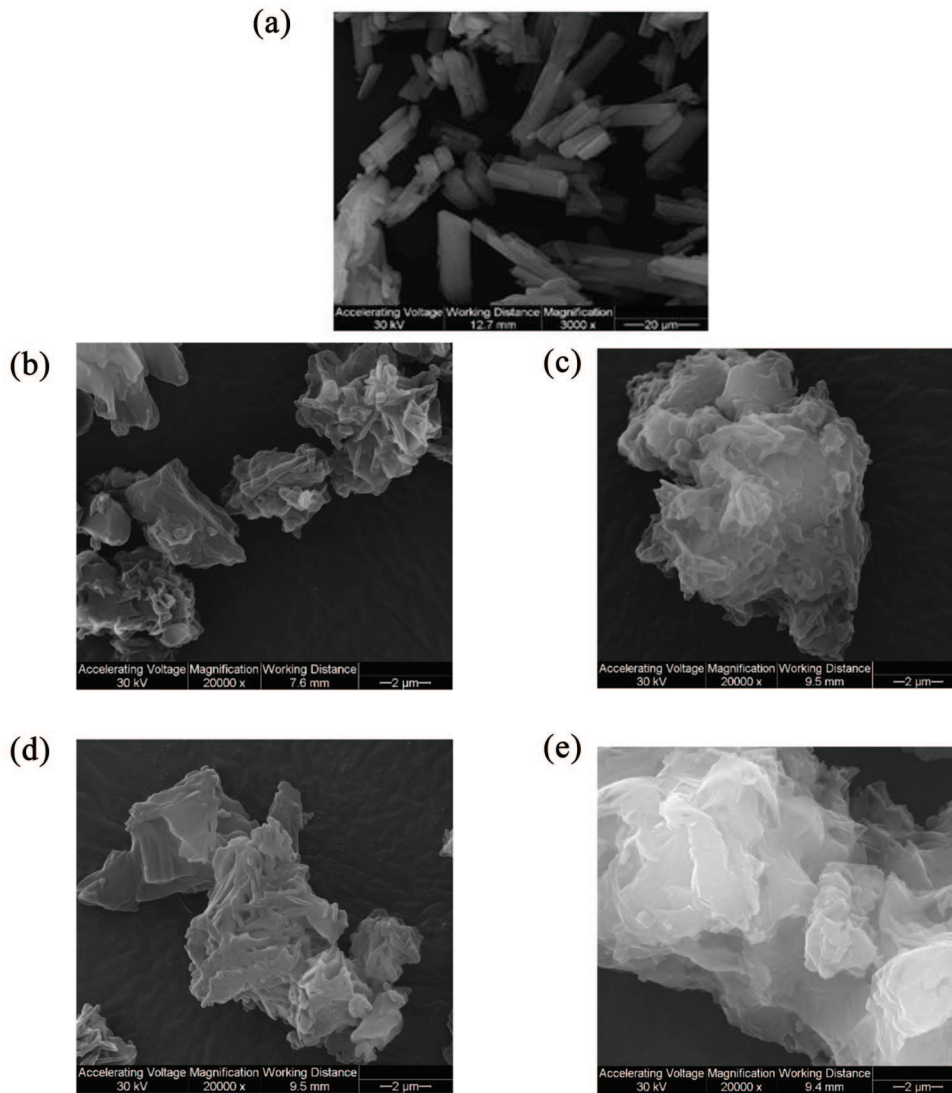


Figure 1. SEM micrographs of raw and SD Sim particles for: (a) raw Sim; (b) 0.1% w/v SD Sim (25% PR); (c) 0.1% w/v SD Sim (50% PR); (d) 0.5% w/v SD Sim (25% PR); and (e) 0.5% w/v SD Sim (50% PR).

Table 3. Particle sizing using image analysis on SEM micrographs ($n \geq 100$ particles).

| System | Mean (μm) | Range (μm) |
|--------------------------|------------------------|-------------------------|
| Raw Sim | 20.063 ± 9.282 | 4.559–29.137 |
| 0.1% w/v SD Sim (25% PR) | 7.84 ± 2.36 | 0.35–13.69 |
| 0.1% w/v SD Sim (50% PR) | 6.59 ± 2.35 | 2.98–18.10 |
| 0.5% w/v SD Sim (25% PR) | 12.64 ± 4.77 | 5.49–28.14 |
| 0.5% w/v SD Sim (50% PR) | 11.77 ± 4.44 | 6.265–32.89 |

PR, pump rate; SD, spray dried; SEM, scanning electron microscopy; Sim, simvastatin.

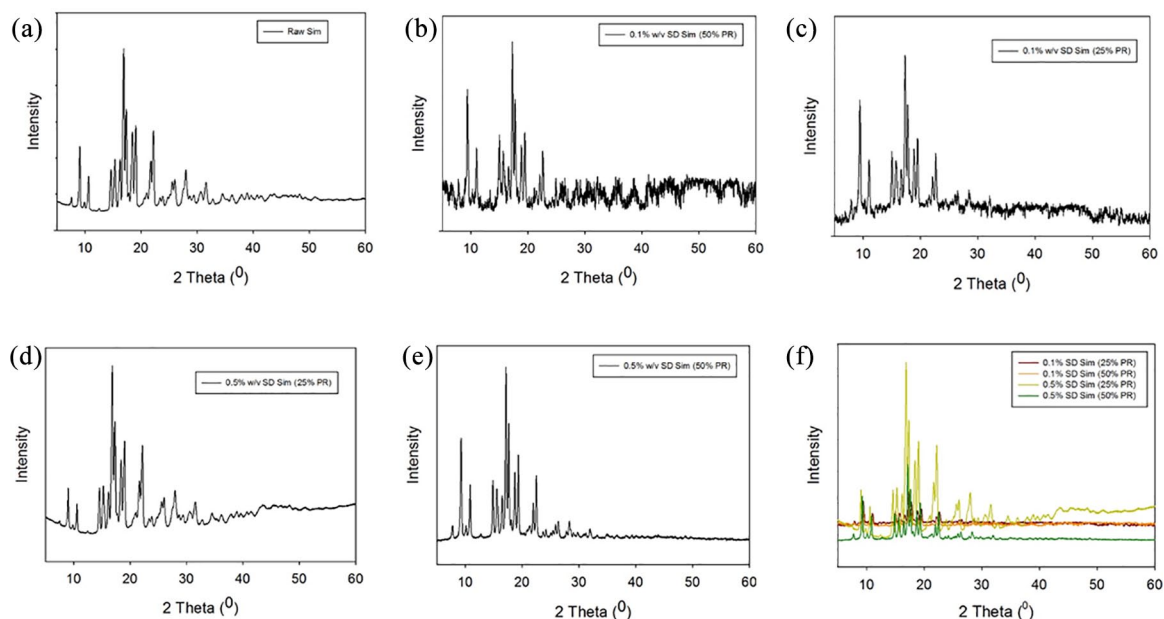


Figure 2. XRPD Diffratograms for: (a) raw Sim; (b) 0.1% w/v SD Sim (25% PR); (c) 0.1% w/v SD Sim (50% PR) (d) 0.5% w/v SD Sim (25% PR); (e) 0.5% w/v SD Sim (50% PR); (f) all.

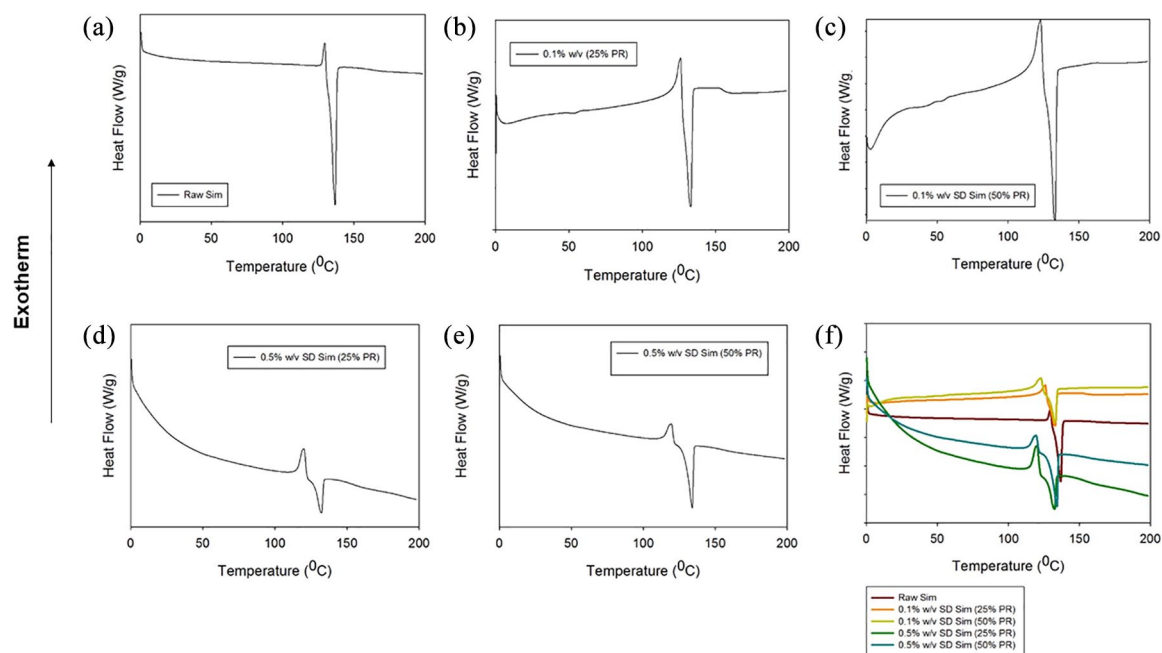


Figure 3. DSC thermograms for: (a) raw Sim; (b) 0.1% w/v SD Sim (25% PR); (c) 0.1% w/v SD Sim (50% PR) (d) 0.5% w/v SD Sim (25% PR); (e) 0.5% w/v SD Sim (50% PR); and (f) all.

HSM under cross-polarizing lens

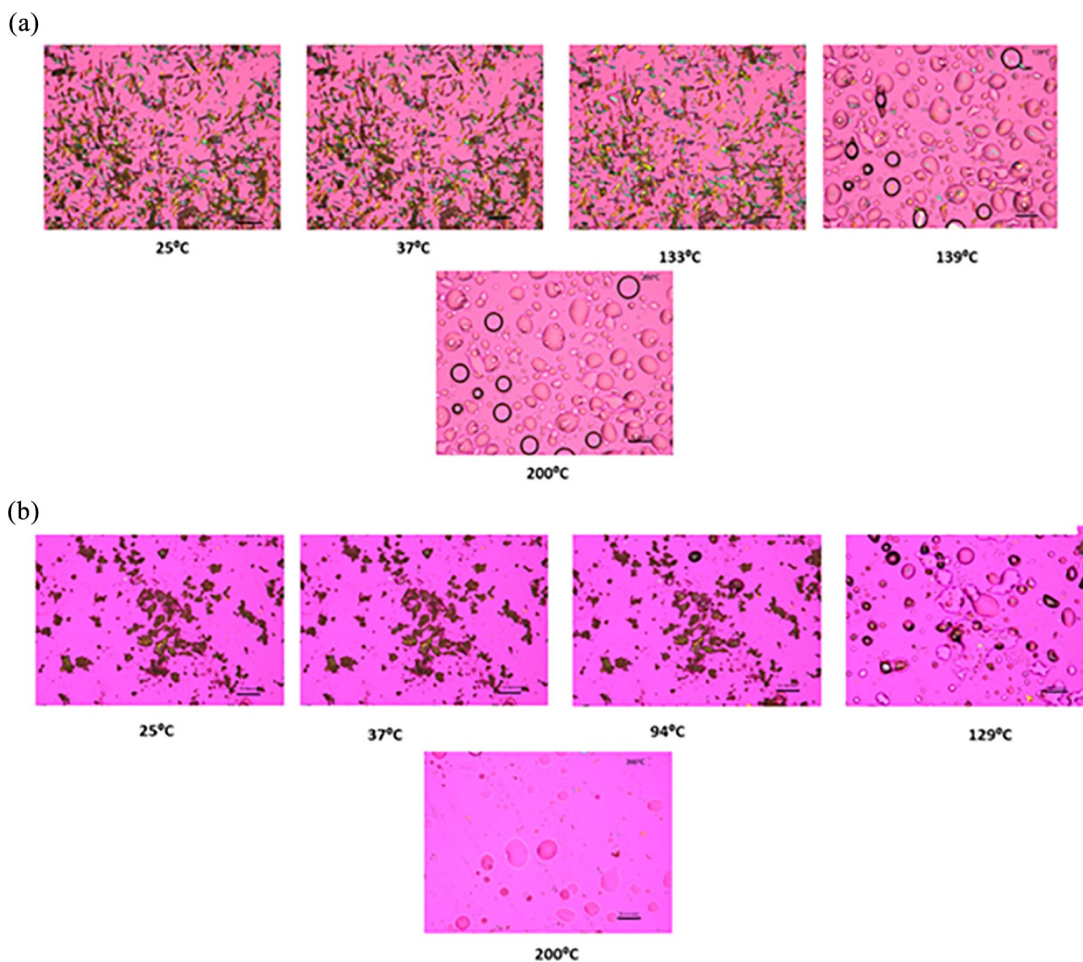
Representative images from the HSM experiment are shown in Figure 4. Raw Sim exhibited birefringence confirming its crystallinity. Raw Sim showed some thermal events before the main thermal event

corresponding to the melting of the drug (i.e. an order-to-disorder phase transition) from the solid state to the liquid state. SD Sim at the different feed concentrations and pump rates was also showing birefringence, which confirms the retention of

Table 4. DSC thermal analysis ($n=3$, mean \pm standard deviation).

| System | Exotherm | | Endotherm | |
|--------------------------|-------------------|------------------|-------------------|------------------|
| | Tpeak (°C) | Enthalpy (J/g) | Tpeak (°C) | Enthalpy (J/g) |
| Raw Sim | 129.50 \pm 0.11 | 5.94 \pm 0.72 | 135.45 \pm 0.06 | 63.24 \pm 0.55 |
| 0.1% w/v SD Sim (25% PR) | 126.05 \pm 0.13 | 6.7 \pm 4.28 | 132.28 \pm 0.44 | 36.96 \pm 3.08 |
| 0.1% w/v SD Sim (50% PR) | 123.41 \pm 0.6 | 10.35 \pm 2.25 | 132.80 \pm 0.13 | 42.73 \pm 4.53 |
| 0.5% w/v SD Sim (25% PR) | 120.69 \pm 0.47 | 31.24 \pm 3.12 | 131.47 \pm 1.02 | 29.75 \pm 6.48 |
| 0.5% w/v SD Sim (50% PR) | 120.08 \pm 0.52 | 22.04 \pm 3.72 | 133.33 \pm 0.8 | 40.39 \pm 6.97 |

DSC, differential scanning calorimetry; PR, pump rate; SD, spray dried; Sim, simvastatin; Tpeak, transition temperature peak.

**Figure 4.** Representative HSM micrographs of: (a) raw Sim and (b) 0.5% w/v SD Sim (25% PR). Scale bar = 10 μ m.

crystallinity after spray drying. Some thermal changes which appeared to be local melting were displayed approximately between 80°C and 100°C

and then the main thermal event at about 125°C corresponding to the melting of the drug where birefringence disappeared, and droplets were

Table 5. Residual water content quantified by coulometric KFT ($n=3$, mean \pm standard deviation).

| System composition | Residual water content (%w/w) |
|--------------------------|-------------------------------|
| Raw Sim | 1.46 ± 0.28 |
| 0.1% w/v SD Sim (25% PR) | 1.16 ± 0.54 |
| 0.1% w/v SD Sim (50% PR) | 1.72 ± 0.59 |
| 0.5% w/v SD Sim (25% PR) | 2.20 ± 0.19 |
| 0.5% w/v SD Sim (50% PR) | 1.46 ± 0.03 |

KFT, karl fischer titration; PR, pump rate; SD, spray dried; Sim, simvastatin.

formed due to the phase transition from solid to liquid. These images were in good agreement with the DSC data previously described.

Karl Fischer titration

The residual water content of all powders was quantified analytically by coulometric KFT, as shown in Table 5. As expected, the residual water content of the powders was very low because Sim was a very hydrophobic drug. The highest residual water content observed was low at approximately 2.20% w/w.

Attenuated total reflectance-FTIR

Formulated particles and their raw counterparts were analyzed by ATR-FTIR to define the functional groups present in the system, as shown in Figure 5. The following bands at the different wavelengths are shown in Figure 5a: 3564 cm^{-1} , 2964 cm^{-1} , 2872 cm^{-1} , 1722 cm^{-1} , 1164 cm^{-1} , 1066 cm^{-1} , which are in good agreement with the literature.⁶⁴ The ATR-FTIR spectra of the SD Sim powders showed the same bands as raw Sim.

Raman spectra

A spectral scan from 100 to $4000/\text{cm}^{-1}$ at 1% laser power and 10 seconds of exposure was performed on all samples to avoid fluorescence. Raman spectra of all raw and SD systems are shown in Figure 6. Raw Sim showed a characteristic Raman shift at 1123 , 1648 and 3074 cm^{-1} , as well as SD Sim at different concentration and pump rates. This was in good agreement with what was previously reported.⁶⁵ Other experimental conditions were tested by increasing the laser power and time of exposure (data not shown); however, fluorescence was predominant in all Sim systems, therefore Raman shifts were not found.

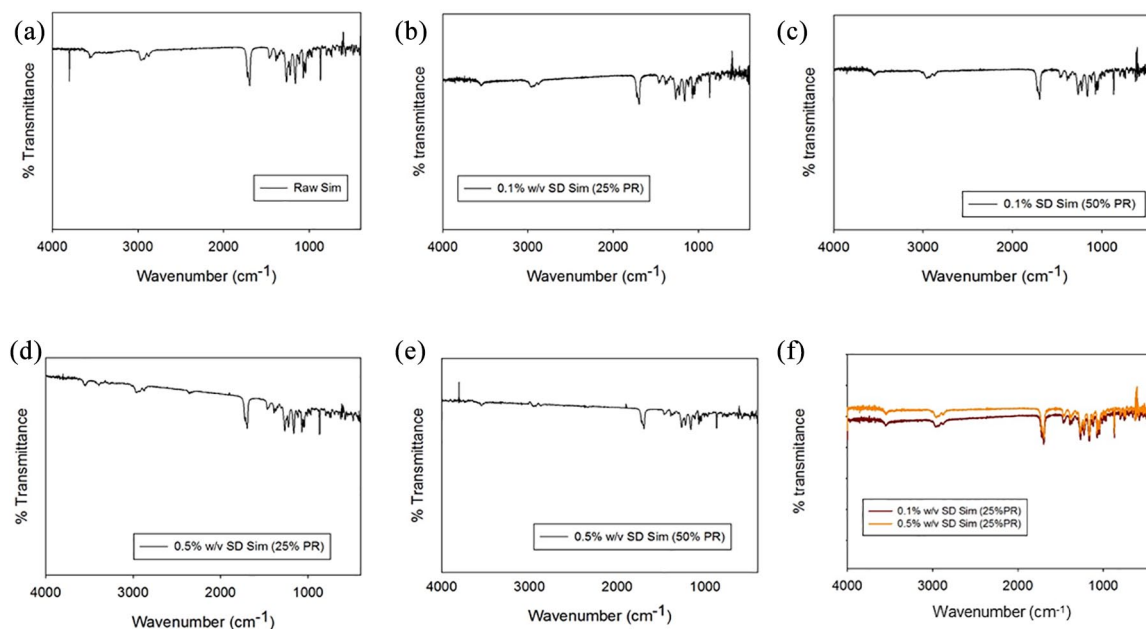


Figure 5. ATR-FTIR spectra for: (a) raw Sim; (b) 0.1% w/v SD Sim (25% PR); (c) 0.1% w/v SD Sim (50% PR) (d) 0.5% w/v SD Sim (25% PR); (e) 0.5% w/v SD Sim (50% PR); (f) all.

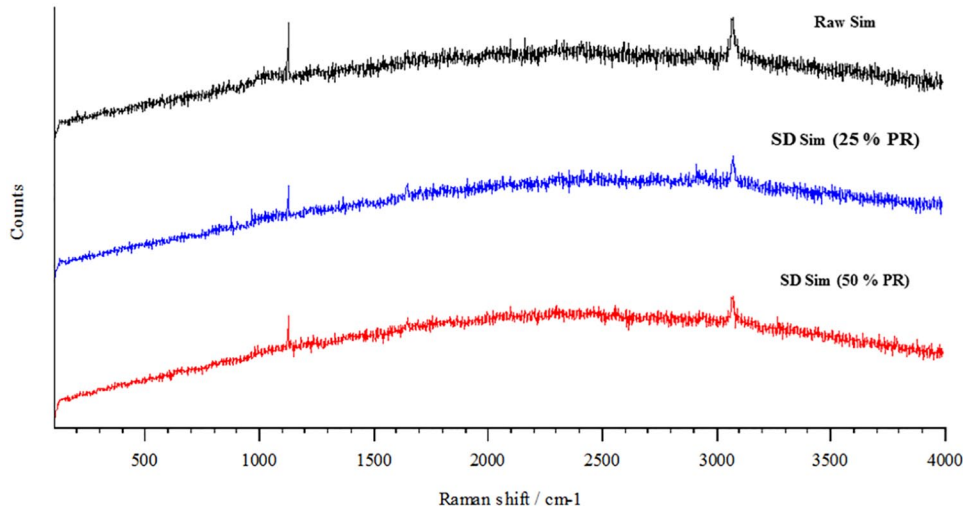


Figure 6. Raman spectra of raw and SD particles for raw Sim, 0.1% w/v SD Sim (25% PR), and 0.5% w/v SD Sim (50% PR).

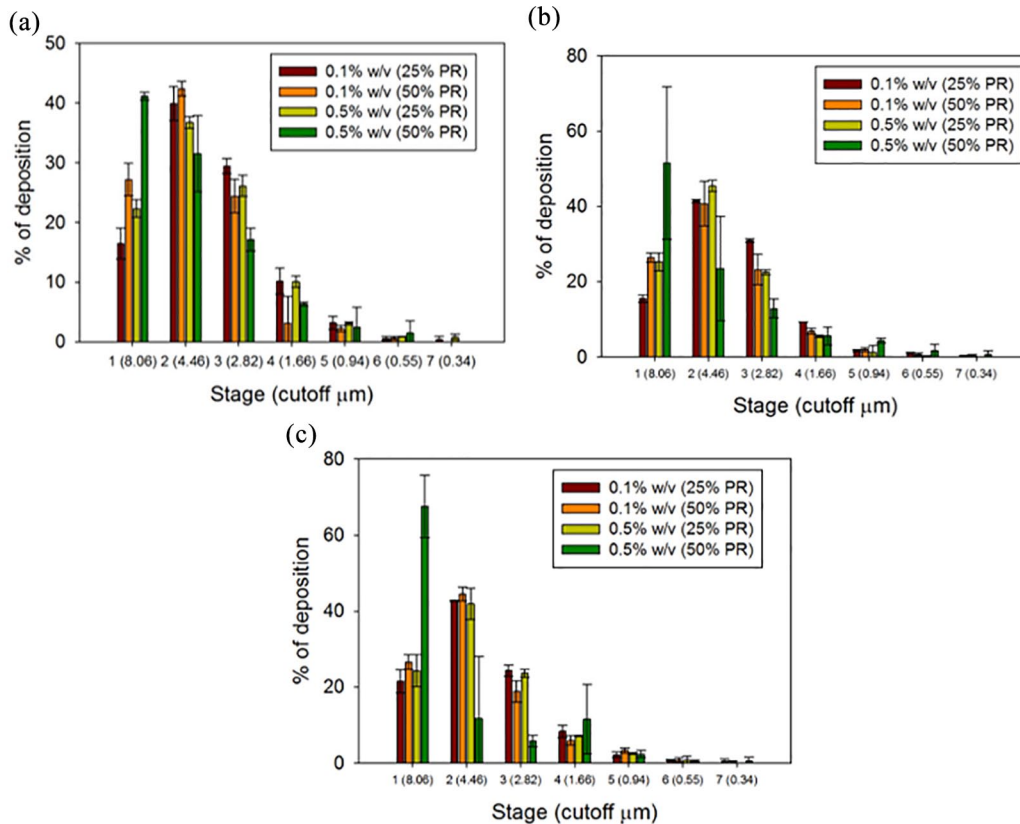


Figure 7. *In Vitro* aerosol deposition using: (a) Aerolizer; (b) NeoHaler; and (c) HandiHaler.

***In vitro* aerosol dispersion performance**

In vitro aerosol dispersion performance was successfully done using the NGI. The particle deposition profiles for each human DPI device is shown in Figure 7. The ED for all four systems with the

three different devices was above 90%. The FPF and the RF percentages were better using medium shear stress (NeoHaler) and high shear stress (HandiHaler) DPI devices. It was evident how the FPF% and the RF% was augmented with the low

Table 6. *In vitro* aerosol dispersion performance using the next generation impactor for SD aerosol systems including MMAD, GSD, ED, FPF, and RF ($n=3$, mean \pm SD).

| System composition | ED (%) | FPF (%) | RF (%) | MMAD (μm) | GSD |
|--------------------------|-------------------|------------------|-------------------|------------------------|------------------|
| Aerolizer | | | | | |
| 0.1% w/v SD Sim (25% PR) | 99.90 \pm 0.14 | 34.15 \pm 0.10 | 83.58 \pm 2.56 | 5.06 \pm 0.23 | 1.7 \pm 0.07 |
| 0.1% w/v SD Sim (50% PR) | 99.14 \pm 0.54 | 24.13 \pm 3.79 | 72.84 \pm 2.70 | 5.85 \pm 0.13 | 1.64 \pm 0.07 |
| 0.5% w/v SD Sim (25% PR) | 99.91 \pm 1.80 | 25.13 \pm 0.55 | 77.69 \pm 1.50 | 7.3 \pm 2.55 | 4.31 \pm 2.55 |
| 0.5% w/v SD Sim (50% PR) | 98.88 \pm 0.96 | 9.16 \pm 1.22 | 58.86 \pm 0.65 | 7.23 \pm 0.17 | 2.29 \pm 0.61 |
| NeoHaler | | | | | |
| 0.1% w/v SD Sim (25% PR) | 99.57 \pm 0.16 | 40.02 \pm 2.95 | 84.53 \pm 1 | 5.00 \pm 0.03 | 1.601 \pm 0.02 |
| 0.1% w/v SD Sim (50% PR) | 98.9 \pm 0.14 | 29.88 \pm 3.36 | 73.65 \pm 1.19 | 6.03 \pm 0.21 | 1.72 \pm 0.21 |
| 0.5% w/v SD Sim (25% PR) | 88.40 \pm 16.40 | 35.39 \pm 6.29 | 74.71 \pm 2.37 | 5.96 \pm 0.08 | 1.65 \pm 0.01 |
| 0.5% w/v SD Sim (50% PR) | 98.84 \pm 0.76 | 12.00 \pm 3.38 | 48.43 \pm 20.2 | 9.9 \pm 3.37 | 2.92 \pm 0.21 |
| HandiHaler® | | | | | |
| 0.1% w/v SD Sim (25% PR) | 98.81 \pm 0.91 | 41.26 \pm 6.62 | 78.262 \pm 6.62 | 5.637 \pm 0.25 | 1.73 \pm 0.02 |
| 0.1% w/v SD Sim (50% PR) | 98.70 \pm 0.81 | 26.62 \pm 0.19 | 73.45 \pm 1.91 | 6.41 \pm 0.35 | 1.79 \pm 0.35 |
| 0.5% w/v SD Sim (25% PR) | 98.7 \pm 0.70 | 30.56 \pm 1.29 | 75.72 \pm 4.19 | 5.83 \pm 0.17 | 1.75 \pm 0.07 |
| 0.5% w/v SD Sim (50% PR) | 98.96 \pm 0.79 | 8.58 \pm 3.86 | 32.44 \pm 8.27 | 19.23 \pm 10.88 | 3.42 \pm 10.88 |

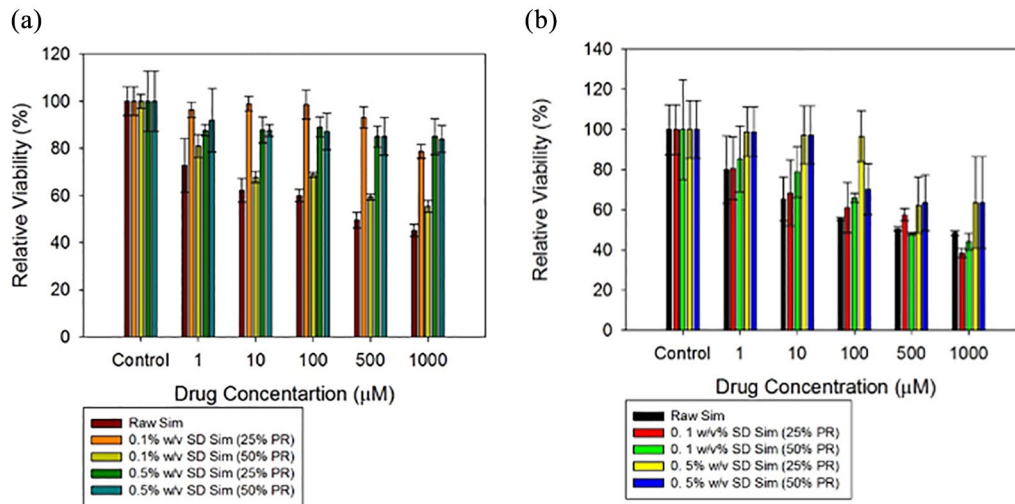
ED, emitted dose; FPF, fine particle fraction; GSD, geometric standard deviation; MMAD, mass median aerodynamic diameter; PR, pump rate; RF, respirable fraction; SD, spray dried; Sim, simvastatin.

FC systems at low PR (0.1% w/v, 25% PR). It was clear that the particle deposition in the lower stages was greater at low FC and low PR using the NeoHaler and the HandiHaler devices. Hence, the MMAD was smaller for this system. It can be said that the performance was reasonable for three of the systems. All parameters were comparable. In contrast, the 0.5% w/v SD Sim 50% PR powder, showed the least optimum aerosol performance parameters, which could be correlated with their physicochemical characteristics. The aerosol dispersion performance parameters for SD Sim using different DPI devices are listed in Table 6.

In vitro cell dose response assay in a 2D cell culture

Different concentrations of raw Sim and the SD Sim formulations were exposed to H358

and A549 cells in order to test the response to this drug. The two different lung cell lines show different relative viability profiles. High cell viability was maintained raw Sim up to 100 μM concentration, while cell viability decreased to 50% and lower for high concentrations of raw Sim at 500 μM and 1000 μM . This trend was seen in both cell lines for raw Sim (Figure 8). The cells were tested at much lower simvastatin concentrations of 0.1 μM , 1 μM , 10 μM , 50 μM and 100 μM (data not shown) and were shown to be safe at 0.1 μM , 1 μM , and 10 μM . However, at concentrations of 50 μM and 100 μM , the relative viability of the cells decreased significantly in comparison with the relative viability of the control cells (no treatment) and the relative viability of the cells exposed to the different formulations (p values $<$ 0.05).



Figures 8. *In vitro* cell viability plots for human pulmonary cell lines: (a) H358 and (b) A549 cells after 72 h of exposure to different concentrations of raw and SD Sim. $n=6$, Mean \pm SD.

In vitro TEER analysis on particle exposure to lung epithelial cells in a 2D cell culture

TEER measurements were successfully performed on Calu-3 cells at ALI conditions to determine the effect of the SD particles on the cell monolayer. The existence of a complete monolayer at ALI was confirmed by TEER values of approximately $500 \Omega/\text{cm}^2$ after 7 days of exposure and by the observance of the monolayer *via* light microscopy (data not shown). As shown in Figure 9, after 3 h of exposure TEER values dropped significantly; however, after 7 days of culturing it was seen that TEER values were approximately $500 \Omega/\text{cm}^2$. Moreover, there was not a statistically significant difference between the TEER values before the drug exposure and after 7 days of cell culturing on each of the formulations (p values > 0.05). It is seen that there is also a significant drop in the TEER values on the control cells. This was due to the aerosols being directly administered right above the monolayer causing a direct disruption that was transient, and therefore a decrease in initial TEER values.

In vitro cell dose response assay in a 3D cell culture at the ALI

As was seen in Figure 10, the exposure of the SmallAir cells at the ALI to $1000 \mu\text{M}$ and $100 \mu\text{M}$ of SD Sim (25% PR) was toxic as the relative viability in both was 0%. By decreasing the Sim

concentration to $50 \mu\text{M}$, the relative viability of the cells increased to almost 60%.

In vitro TEER analysis upon particle exposure to 3D human small airway epithelia

The same trend was observed by measuring TEER after the exposure of the cells to SD Sim (25%

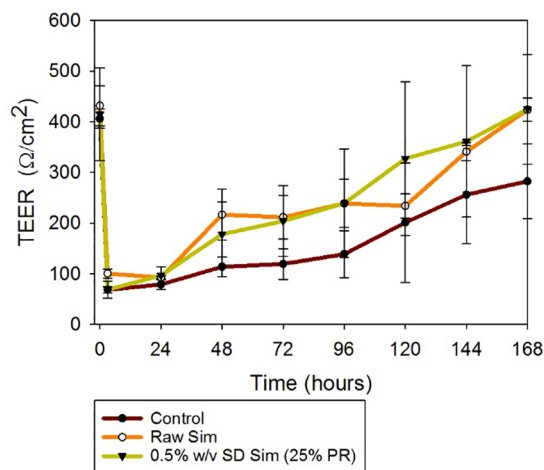
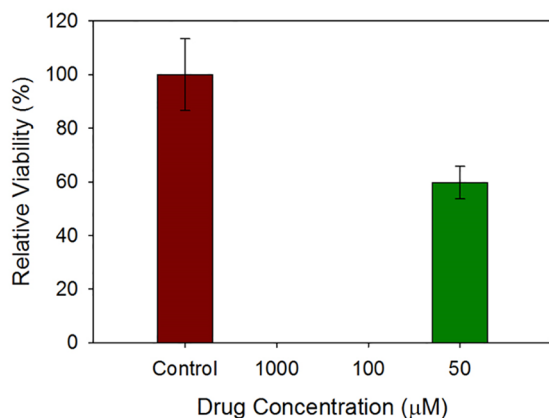
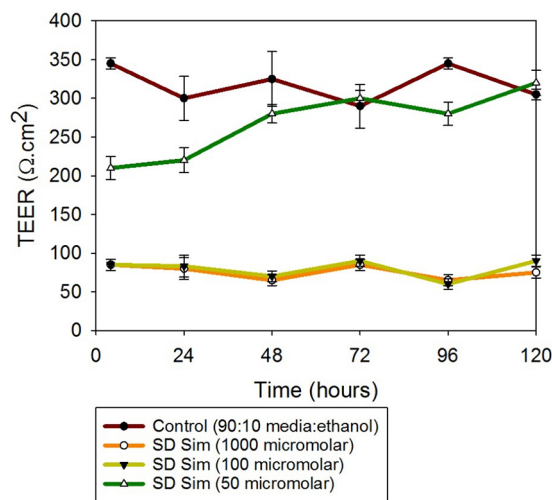


Figure 9. Transepithelial electrical resistance (TEER) analysis of Calu-3 human lung epithelial cells exposed to $100 \mu\text{M}$ of raw and SD Sim in air-liquid interface (ALI) conditions, using the Penn Century MicroSprayer Aerolizer (Penn Century, Inc., Wyndmoor, PA, USA). $n=3$, mean \pm SD.



Figures 10. *In vitro* viability of SmallAir 3D human pulmonary epithelia composed of primary cells at the ALI after 72 h of exposure to different concentrations of SD Sim. $n=3$, Mean \pm SD.



Figures 11. Transepithelial electrical resistance (TEER) analysis of SmallAir 3D human pulmonary epithelia composed of primary cells at the ALI exposed to different concentrations of SD Sim using a micropipette. $n=3$, mean \pm SD.

PR). When the cells were exposed to 1000 μM and 100 μM Sim, the TEER values were below 100 Ω/cm^2 and they did not recover with time. After decreasing the concentration to 50 μM , the TEER values were above 200 Ω/cm^2 . These results are observed in Figure 11. In contrast with the TEER experiment in the 2D model at the ALI, the formulations were added with a micropipette; hence, the disruption of the monolayer for the control cells was not as evident.

Enzyme-linked immunosorbent assay

As shown in Figure 12a, two important biomarkers for PH were measured in BALF biosamples by ELISA. For IL-6, there was a statistically significant difference between the control and the treated groups, namely a reduction in BALF IL-6 in the inhaled SD Sim rat groups. For TNF- α , there was a statistically significant difference between the control and the SD Sim-treated groups, namely an increase in the BALF TNF- α in the inhaled SD Sim rat group.

Histological analysis

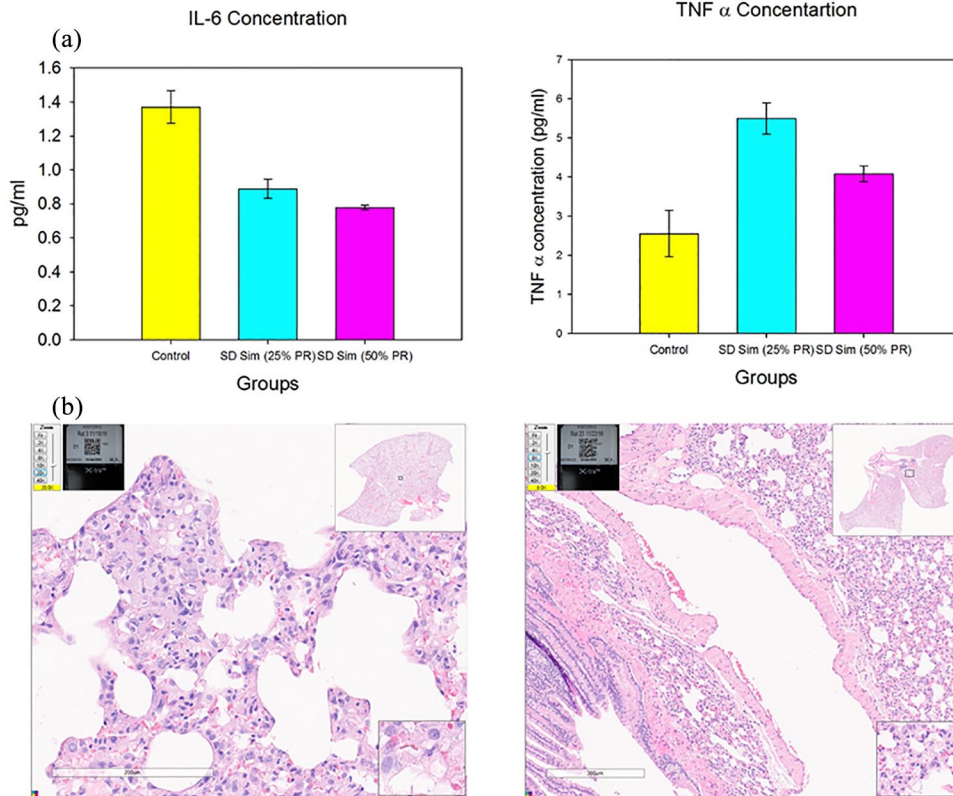
In the H&E images showed in Figure 12b, there was no evidence of inflammatory cells, excessive proliferation of cells, remodeling of vessels, injuries or other signs of damage. The images showed healthy lungs.

Efficacy study in the *in vivo* shunt lamb model of PH

Prior to inhaled Sim, systemic administration of the endothelium-dependent vasodilator acetylcholine decreased mean systemic arterial pressure from 44.5 to 32.0 mmHg, while mean pulmonary arterial pressure did not change (22.2–21.0 mmHg). Administration of inhaled Sim did not change hemodynamics (mean pulmonary artery pressure went from 25.1 to 25.2). One hour following inhaled Sim administration, both systemic (from 37.6 to 31.7 mmHg) and pulmonary arterial pressure (from 25.2 to 21.6 mmHg) decreased. Changes in pulmonary vascular resistance tracked changes in pulmonary arterial pressure (Figure 13). Thus, inhaled Sim as an aerosol restored the endothelial function in the shunt lamb model of PH, as demonstrated by the reduction of PVR in response to the endothelium-dependent vasodilator acetylcholine. At baseline, shunt lambs do exhibit a pulmonary vasodilator response to acetylcholine (Figure 13, pre bar). However, after pulmonary administration of inhaled simvastatin the pulmonary vasodilator response to acetylcholine is restored (Figure 13, post bar). Both measurements were conducted in response to the vasoconstrictor acetylcholine that occurred 1 hour after delivery (Figure 13, post bar).

Discussion

To our knowledge, there are several significant new findings reported in this systematic study. This was the first time that Sim was formulated as



Figures 12. (a) IL-6 and TNF- α concentration in BALF samples of rats; (b) H&E images of healthy rat lungs following inhalation delivery.

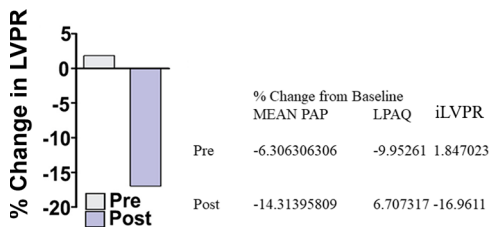


Figure 13. *In vivo* efficacy study in the shunt lamb model of PH following inhaled simvastatin.

a DPI employing organic solution advanced closed-mode spray drying under the reported conditions. The comprehensive physicochemical characterization and the *in vitro* aerosol dispersion performance were completed along with *in vitro* human lung cell culture demonstrating safety, *in vivo* safety in rats of inhaled Sim, and efficacy of inhaled Sim in a shunt lamb model of PH. Our data demonstrate that inhaled Sim is safe and effectively and efficiently treats PH. In order to achieve this, it was necessary for the particles to have an optimal aerosol performance and

reach the smaller airways (i.e. bronchiolar region) and peripheral lung regions.^{47,55,66} Decreasing the interparticulate interactions to a minimum led to high FPF values. On the other hand, structural cohesion and aggregation due to interparticulate interactions such as van der Waals forces, capillary forces, electrostatic forces, and mechanical interlocking avoided the proper aerosolization of the powder and led to low FPF values.

Particle characteristics such as morphology, size, surface, density, and residual water content are of importance in the development of therapeutic powder aerosol formulations and were manipulated depending on the desirable formulation and the parameters employed in spray drying.⁶⁷ In this study, the formation of particles was only achieved at low and medium pump rates (25% and 50%) in the two designed systems 0.1% w/v and 0.5%w/v, although higher pump rates (75% and 100%) were also tried with no success. Equivalent sphere shape and slightly wrinkled surface were achieved in all SD systems as was seen in SEM micrographs (Figure 1). Nanostructures

were clearly perceived in the surface of the particles leading to their aggregation. This occurrence made it difficult to size the particles using SigmaScan. It is important to mention that the 0.1% w/v SD systems at both PR were within the respirable size $\leq 8\mu\text{m}$.^{68,69} All powders contained very low residual water content (Table 2), as expected due to the hydrophobicity of Sim and also due to the advanced spray drying process from organic solution in closed mode. All these values were acceptable for dry powder inhalation aerosol formulations.⁷⁰

Aggregation of particles gave large geometric mean diameter, large and broad particle size distribution. Although corrugated or wrinkled particles had larger surface area than spherical particles, the asperity of their surface decreased the surface area of true contact between particles leading to a decrease of cohesive forces between them.⁶⁷ This phenomenon explained the optimum aerosol dispersion performance and the small MMAD values for some of the systems, although the SEM micrographs were showing aggregates and large particles.

The aerosol deposition properties (Figure 7 and Table 6) showed measurable and significant stage deposition on the lower stages with smaller aerodynamic D_{50} cut-off values much smaller than 8 microns, which were achieved as a function of the composition and nanostructure of the particles. High ED and FPF values were achieved in three of the systems. The low residual water content in all the systems also played a role in this high deposition. For inhalable powders, residual water in the powder needs to be minimized as it has significant effects on aerosol dispersion, particle size distribution, crystallinity, and stability. It is well known that reducing the residual content directly reduces capillary forces. After spray drying the residual water content was not increased, despite the pump rate. In general, particles formed at low pump rates showed more spherical shape, less wrinkled surface, and less residual water content. This trend occurred because at lower pump rates there was more time for particle formation and for drying in both the primary and secondary drying chambers during the spray drying process. In general, better aerosolization was achieved at lower pump rates of all SD. Regarding the device aspect, there was a better aerosol dispersion performance using medium and high resistance

devices. The resistance of the device helped the de-aggregation of the particles and hence their deposition in the lower stages of the NGI.

The process parameter interaction plot and 3D surface response graphs generated for the different SD Sim systems from Design-Expert software are shown in Figures 14–16. The interaction between feed solution concentration and spray drying pump rate using different DPI devices was studied using one-way ANOVA analysis. The statistical test showed that RF, FPF presented a statistically significant difference, whereas the ED and MMAD values did not show a statistically significant difference.

Retention of crystallinity after spray drying was demonstrated in all SD systems. XRPD diffraction patterns showed sharp peaks in all powders which are indicative of the long-range molecular order (Figure 2) characteristic of crystalline organic materials. DSC thermograms (Figure 3) also confirmed the presence of crystalline structures in all SD systems. Fast DSC heating scans were conducted at 20°C/min and 40°C/min on the raw and SD Sim powders and no T_g was detected (data not shown). This suggested that the powders were crystalline and retained crystallinity after advanced spray drying under these conditions which agreed well with the XRPD diffractograms. As no T_g was detected with fast DSC heating scans but there was an exotherm present before melting in raw Sim and SD Sim in the thermograms, a solid–solid phase transition (polymorphic interconversion from a higher delta G polymorph to a lower delta G polymorph) is likely. This is consistent with previous reports that showed different polymorphs of Sim.⁷¹ As seen in the DSC thermograms, this polymorphic interconversion was observed at approximately 120°C. The decrease in peak intensity is observed in the XRPD diffractograms and the decrease in the enthalpies from the DSC thermograms suggested a change in the crystallinity of Sim after spray drying under these conditions.

HSM (Figure 4) enabled the visualization of the particles as a function of temperature and confirmed the phase transitions of the formulated particles. It also demonstrated the stability of the particles at room and physiological temperatures. The local melting observed in SD Sim was suggestive of having nanodomains which was in good

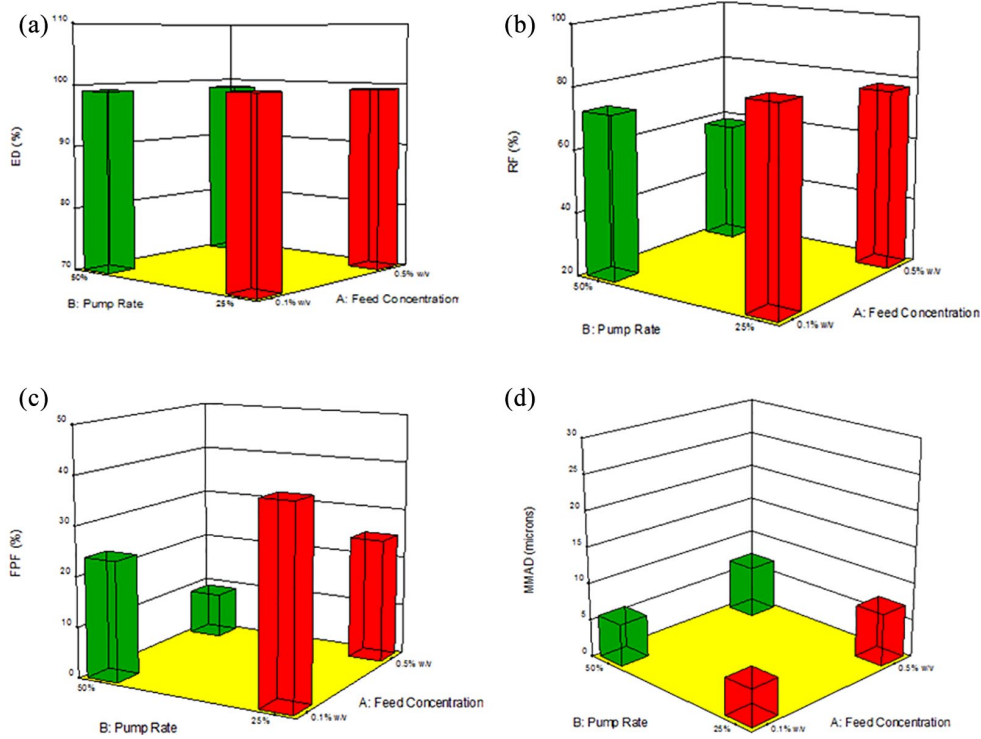


Figure 14. 3D surface response plots showing the influence of feed solution concentration, spray drying pump rate using the Aerosolizer DPI device on *in vitro* aerosol dispersion performance for SD Sim formulations for (a) ED; (b) RF; (c) FPF; and (d) MMAD.

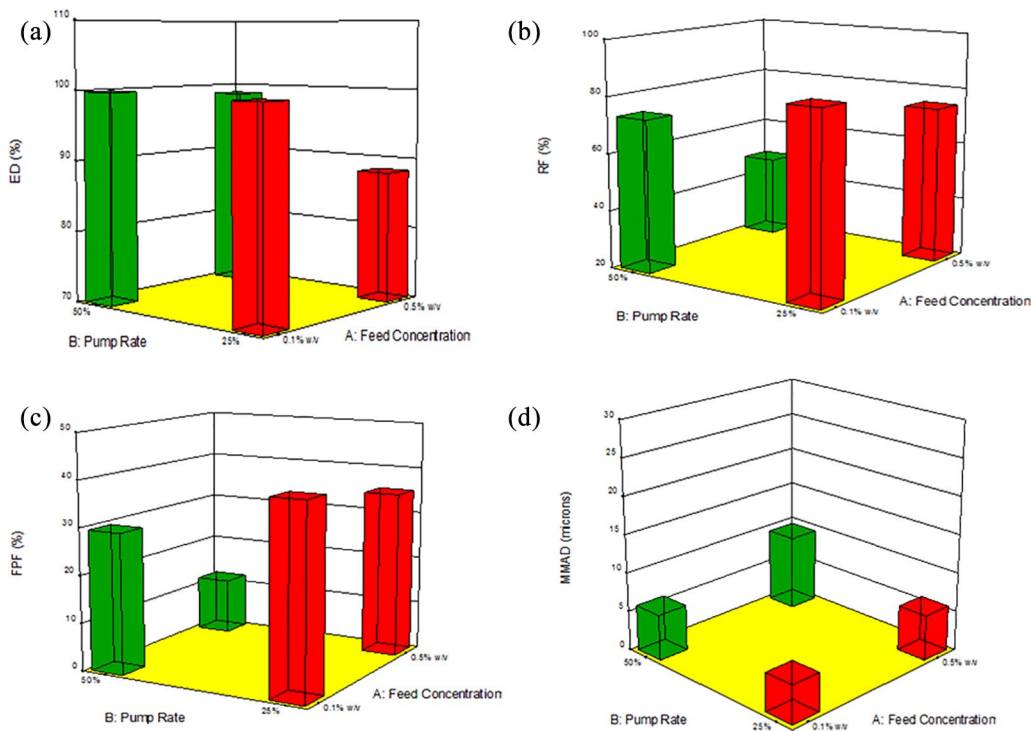


Figure 15. 3D surface response plots showing the influence of feed solution concentration, spray drying pump rate using the NeoHaler DPI device on *in vitro* aerosol dispersion performance for SD Sim formulations for (a) ED; (b) RF; (c) FPF; and (d) MMAD.

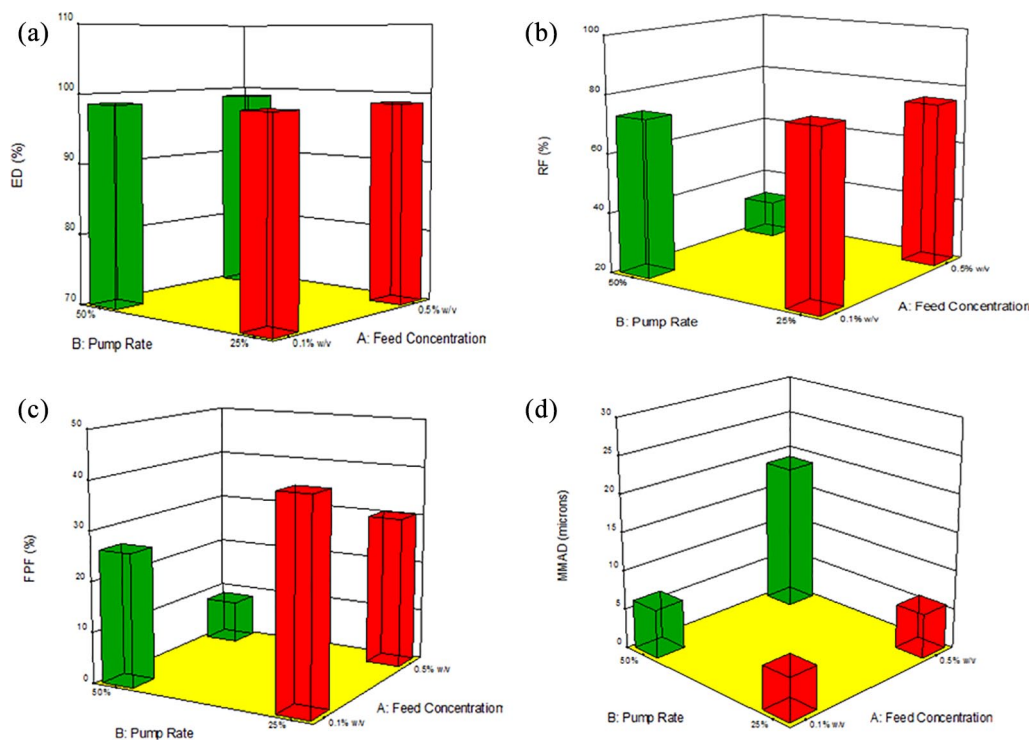


Figure 16. 3D surface response plots showing the influence of feed solution concentration, spray drying pump rate using the HandiHaler DPI device on *in vitro* aerosol dispersion performance for SD Sim formulations for (a) ED; (b) RF; (c) FPF; and (d) MMAD.

agreement with SEM micrographs. Birefringence confirmed the crystallinity of raw and SD powders as well.

Raman spectroscopy and ATR-FTIR provided non-invasive and non-destructive microspectroscopic ‘molecular fingerprinting’ component analysis of DPI formulations. ATR-FTIR spectra of raw Sim and SD Sim, as seen in Figure 5, were identical. This confirmed that Sim was not degraded or did not have any change during the spray drying process. Characteristic infrared absorptions corresponding to the functional groups present in the Sim molecule were identified: OH vibration was identified at 3547 cm^{-1} ; CH vibration was identified at 2965 cm^{-1} ; and the stretch vibration of the C–O and C=O was identified at 1722 , 1163 and 1066 cm^{-1} , in both raw and SD systems. This was in good agreement with the literature.⁶⁴ The characteristic Raman shifts of Sim (Figure 6) were found in the $3200\text{--}2800\text{ cm}^{-1}$ region and at 1650 cm^{-1} , which were related to the C–H and ester, lactone group vibrations, respectively.⁶⁵ These peaks were consistent

in both raw and SD systems, meaning that Sim was not degraded or interconverted after spray drying.

In vitro cell analysis as 2D cell culture and 3D human pulmonary cell culture at the ALI all confirmed that these formulations maintained cell viability and were biocompatible at different concentrations, but also presented a reduction in cell viability at certain high concentrations.

The integrity of a cell monolayer was evaluated by measuring the TEER of Calu-3 large airway bronchial epithelial cells at the ALI (Figure 9). TEER reduction had been used as an indication of adverse effects of model toxicants and inhaled delivery vehicles and these results corresponded well with standard toxicological tests.^{50,55,57} Calu-3 (bronchial lung cancer cell line) was used as a representative model of the airway epithelial barrier. When grown using ALI, the lung cell layers resembled the native epithelium to a greater extent than cells grown in media in which the cells display enhanced ciliogenesis, increased

mucus secretion, and more physiological TEER values.⁵⁵ Right after treatment, a decrease in TEER values was visible due to the delivery method directly on the cells. However, it was clear that after a few days this monolayer recovered, and the tight junctions were formed again.

The *in vitro* viability (Figure 10) and TEER assays (Figure 11) done using SmallAir 3D cells at the ALI clearly showed a dose-dependent effect. The cells were very sensitive to Sim, meaning that low amounts of drug must be used in order to avoid toxicity and have a desired effect. This result was expected, as SmallAir cells were primary cells taken from diseased patients, so they were more sensitive to the drug formulations than the immortal cell line (CaLu-3).

The two BALF biomarkers and the immunopathology showed that there was no damage after the aerosolization of the SD powders in healthy rats. There were no signals of injuries in the H&E images and the biomarker concentration in BALF was about the same as in the control animals. These two biomarkers were measured because they were indicative of some alteration that can lead to PH.⁷²

For the *in vivo* efficacy study in the validated shunt lamb model of PH, it was shown that acetylcholine induced vasoconstriction in shunt lambs at 4 weeks of age prior to simvastatin lung delivery. However, after the aerosol delivery of simvastatin (6.5 mg/kg) to the ovine lung, vasodilation was enhanced, decreasing the pulmonary arterial pressure (PAP) of the lambs. A future *in vivo* efficacy study would be in the monocrotaline (MCT) rat model of PH, a validated rodent model of PH, which would have a different study design.

Conclusions

Dry powder aerosol powders of simvastatin were successfully designed for inhalation by particle engineering design technology using organic solution advanced spray drying from two different dilute solute concentrations and at two spray drying pump rates. Comprehensive physicochemical characterization revealed that simvastatin retains crystallinity (long-range molecular order) and the solid state particles formed were microparticles with nanostructure surfaces following advanced spray drying under these conditions. This RhoA/ROCK inhibitor and Nrf2 activator has promising potential to

treat complex pulmonary diseases such as PH. *In vitro* aerosol dispersion performance demonstrated that all the spray dried powders aerosolized with all three DPI human devices and gave high aerosol performance parameters. *In vitro* 2D cell viability under LLC and 3D human lung small airway epithelia composed of primary cells at the ALI demonstrated cell viability and biocompatibility as a function of drug dose. The *in vivo* inhalation studies performed in rats successfully demonstrated safety, biocompatibility, and efficacy was successfully demonstrated in a validated diseased animal model of PH in a shunt lamb which clearly showed that inhaled simvastatin effectively treated PH in a validated lamb model of PH.

Acknowledgements

All SEM images and data were collected in the W.M. Keck Center for Nano-Scale Imaging in the Department of Chemistry and Biochemistry at the University of Arizona with funding from the W.M. Keck Foundation grant. The authors thank the Imaging Cores Materials Imaging and Characterization Facility supported by the University of Arizona Office of Research, Discovery and Innovation and the X-ray diffraction facility of the Department of Chemistry and Biochemistry at the University of Arizona. This material is based on work supported by the National Science Foundation under grant number #0619599 and Arizona Proposition 301: Technology and Research Initiative Fund (A.R.S.§15-1648). The authors sincerely thank Brooke Beam-Massani, Paul Wallace, Andrei Astachkine, and Chad Park for core facility access and assistance. Thanks to SMB laboratory and personal for their assistance with the animal studies. The authors gratefully acknowledge the CONACyT (National Council of Science and Technology of Mexico) fellowship awarded to MFA. This work was supported by 1R01HL137282 (HMM, SMB, and JRF), R01HL60190 (SMB), R21AG054766 (HMM), R21AI135935 (HMM and SMB), P01HL146369 (SMB and JRF), and P01HL103453 (HMM).

Author contributions

HMM SMB JRF DHJr (study project conception, study project design, experiments, data analysis, interpretation, manuscript write-up/review/editing). MFA, PM, CLG, MDA (experiments, data analysis, interpretation, manuscript write-up/review/editing).

Funding

The authors disclosed receipt of the following financial support for the research, authorship, and/or publication of this article: This work was supported by 1R01HL137282 (HMM, SMB, and JRF), R01HL60190 (SMB), R21AG054766 (HMM), R21AI135935 (HMM and SMB), P01HL146369 (SMB and JRF), and P01HL103453 (HMM). This material is based on work supported by the National Science Foundation under grant number #0619599 and Arizona Proposition 301: Technology and Research Initiative Fund (A.R.S.§15-1648).

NIH 1R01HL137282, NIH R01HL60190, NIH R21AG054766, NIH R21AI135935, NIH P01HL146369 and NIH P01HL103453, CONACyT Fellowship, NSF #0619599, Arizona Proposition 301: Technology and Research Initiative Fund (A.R.S.§15-1648).

Conflict of interest statement

The authors declare that there is no conflict of interest.

Ethical approval

Not applicable.

Consent to participate

Not applicable.

Consent to publish case report

Not applicable.

Guarantor

Not applicable.

ORCID iD

Heidi M. Mansour  <https://orcid.org/0000-0003-3993-9210>

Supplemental material

The reviews of this paper are available via the supplemental material section.

References

- de Jesus Perez VA. Molecular pathogenesis and current pathology of pulmonary hypertension. *Heart Fail Rev* 2016; 21: 239–257.
- Gan CT, Noordegraaf AV, Marques KMJ, *et al.* A review of pulmonary arterial hypertension. Part

1: Novel insights and classification. *Neth Heart J* 2004; 12: 287–294.

- Acosta MF, Hayes DJ, Fineman JR, *et al.* Chapter 19: Therapeutics in pulmonary hypertension. In: Hickey AJ and Mansour HM (eds) *Inhalation aerosols: physical and biological basis for therapy*, 3rd ed. London: CRC Press/Taylor & Francis, 2019, pp. 313–322.
- Oishi P and Fineman JR. Pulmonary hypertension. *Pediatr Crit Care Med* 2016; 17 (Suppl. 1): S140–S145.
- Hayes D Jr, Black SM, Tobias JD, *et al.* Prevalence of pulmonary hypertension and its influence on survival in patients with advanced chronic obstructive pulmonary disease prior to lung transplantation. *COPD* 2016; 13: 50–56.
- Hayes D Jr, Tobias JD, Mansour HM, *et al.* Pulmonary hypertension in cystic fibrosis with advanced lung disease. *Am J Respir Crit Care Med* 2014; 190: 898–905.
- Hayes D Jr, Black SM, Tobias JD, *et al.* Influence of pulmonary hypertension on survival in advanced lung disease. *Lung* 2015; 193: 213–221.
- Hayes D Jr, Tumin D, Daniels CJ, *et al.* Pulmonary artery pressure and benefit of lung transplantation in adult cystic fibrosis patients. *Ann Thorac Surg*. Epub ahead of print 11 December 2015. DOI: 10.1016/j.athoracsur.2015.09.086
- Muralidharan P, Hayes DJ and Mansour HM. Chapter 18: Pulmonary fibrosis. In: Hickey AJ and Mansour HM (eds) *Inhalation aerosols: physical and biological basis for therapy*, 3rd ed. London: CRC Press/Taylor & Francis, 2019, pp. 303–312.
- Hayes D Jr, Black SM, Tobias JD, *et al.* Influence of pulmonary hypertension on patients with idiopathic pulmonary fibrosis awaiting lung transplantation. *Ann Thorac Surg* 2016; 101: 246–252.
- Iqbal M, Cawthon D, Wideman RF Jr, *et al.* Lung mitochondrial dysfunction in pulmonary hypertension syndrome. II. Oxidative stress and inability to improve function with repeated additions of adenosine diphosphate. *Poult Sci* 2001; 80: 656–665.
- Kellner M, Noonepalle S, Lu Q, *et al.* ROS signaling in the pathogenesis of Acute Lung Injury (ALI) and Acute Respiratory Distress Syndrome (ARDS). In: Wang Y-X (ed.) *Pulmonary vasculature redox signaling in health and disease*. Cham: Springer International Publishing, 2017, pp. 105–137.

13. Liao JK, Seto M and Noma K. Rho kinase (ROCK) inhibitors. *J Cardiovasc Pharmacol* 2007; 50: 17–24.
14. Rikitake Y and Liao JK. Rho GTPases, statins, and nitric oxide. *Circ Res* 2005; 97: 1232–1235.
15. Zhang Z, Wang M, Xue S-J, *et al.* Simvastatin ameliorates angiotensin II-induced endothelial dysfunction through restoration of Rho-BH4-eNOS-NO pathway. *Cardiovasc Drugs Ther* 2012; 26: 31–40.
16. Katsiki N, Wierzbicki AS and Mikhailidis DP. Pulmonary arterial hypertension and statins: an update. *Curr Opin Cardiol* 2011; 26: 322–326.
17. Zhao L, Sebkhii A, Ali O, *et al.* Simvastatin and sildenafil combine to attenuate pulmonary hypertension. *Eur Respir J* 2009; 34: 948–957.
18. Taraseviciene-Stewart L, Scerbavicius R, Choe K-H, *et al.* Simvastatin causes endothelial cell apoptosis and attenuates severe pulmonary hypertension. *Am J Physiol Lung Cell Mol Physiol* 2006; 291: L668–L676.
19. Nishimura T, Faul JL, Berry GJ, *et al.* Simvastatin attenuates smooth muscle neointimal proliferation and pulmonary hypertension in rats. *Am J Respir Crit Care Med* 2002; 166: 1403–1408.
20. Girgis RE, Mozammel S, Champion HC, *et al.* Regression of chronic hypoxic pulmonary hypertension by simvastatin. *Am J Physiol Lung Cell Mol Physiol* 2007; 292: L1105–L1110.
21. Lee DS, Kim YK and Jung YW. Simvastatin, sildenafil and their combination in monocrotaline-induced pulmonary arterial hypertension. *Korean Circ J* 2010; 40: 659–664.
22. Kuang T, Wang J, Pang B, *et al.* Combination of sildenafil and simvastatin ameliorates monocrotaline-induced pulmonary hypertension in rats. *Pulm Pharmacol Ther* 2010; 23: 456–464.
23. Girgis RE, Li D, Zhan X, *et al.* Attenuation of chronic hypoxic pulmonary hypertension by simvastatin. *Am J Physiol Heart Circ Physiol* 2003; 285: H938–H945.
24. Nishimura T, Vaszar LT, Faul JL, *et al.* Simvastatin rescues rats from fatal pulmonary hypertension by inducing apoptosis of neointimal smooth muscle cells. *Circ Res* 2003; 108: 1640–1645.
25. Kao PN. Simvastatin treatment of pulmonary hypertension: an observational case series. *Chest* 2005; 127: 1446–1452.
26. Lee JH, Lee DS, Kim EK, *et al.* Simvastatin inhibits cigarette smoking-induced emphysema and pulmonary hypertension in rat lungs. *Am J Respir Crit Care Med* 2005; 172: 987–993.
27. Mathew B, Huang Y, Jacobson JR, *et al.* Simvastatin attenuates radiation-induced murine lung injury and dysregulated lung gene expression. *Am J Respir Cell Mol Biol* 2011; 44: 415–422.
28. Habeos IG, Ziros PG, Chartoumpekis D, *et al.* Simvastatin activates Keap1/Nrf2 signaling in rat liver. *J Mol Med (Berl)* 2008; 86: 1279–1285.
29. Jang HJ, Hong EM, Kim M, *et al.* Simvastatin induces heme oxygenase-1 via NF-E2-related factor 2 (Nrf2) activation through ERK and PI3K/Akt pathway in colon cancer *Oncotarget* 2016; 7: 46219–46229.
30. Chartoumpekis D, Ziros PG, Psyrogiannis A, *et al.* Simvastatin lowers reactive oxygen species level by Nrf2 activation via PI3K/Akt pathway. *Biochem Biophys Res Commun* 2010; 396: 463–466.
31. Zhang Y, Rong S, Feng Y, *et al.* Simvastatin attenuates renal ischemia/reperfusion injury from oxidative stress via targeting Nrf2/HO-1 pathway. *Exp Ther Med* 2017; 14: 4460–4466.
32. Rojo de la Vega M, Dodson M, Gross C, *et al.* Role of Nrf2 and autophagy in acute lung injury. *Curr Pharmacol Rep* 2016; 2: 91–101.
33. Vallorz E, Sheth P and Myrdal P. Pressurized metered dose inhaler technology: manufacturing. *AAPS PharmSciTech* 2019; 20: 177.
34. Myrdal PB, Sheth P and Stein SW. Advances in metered dose inhaler technology: formulation development. *AAPS PharmSciTech* 2014; 15: 434–455.
35. Stein SW, Sheth P, Hodson PD, *et al.* Advances in metered dose inhaler technology: hardware development. *AAPS PharmSciTech* 2014; 15: 326–338.
36. Hickey AJ and Mansour HM. Chapter 43: Formulation challenges of powders for the delivery of small molecular weight molecules as aerosols. In: Rathbone MJ, Hadgraft J, Roberts MS, *et al.* (eds) *Modified-release drug delivery technology*, 2nd ed. New York: Informa Healthcare, 2008, pp. 573–602.
37. Muralidharan P, Hayes D Jr and Mansour HM. Dry powder inhalers in COPD, lung inflammation and pulmonary infections. *Expert Opin Drug Deliv* 2015; 12: 947–962.
38. Telko MJ and Hickey AJ. Dry powder inhaler formulation. *Respir Care* 2005; 50: 1209–1227.

39. Yang MY, Chan JG and Chan H-K. Pulmonary drug delivery by powder aerosols. *J Control Release* 2014; 193: 228–240.
40. Mansour HM. Inhaled medical aerosols by nebulizer delivery in pulmonary hypertension. *Pulm Circ* 2018; 8: 2045894018809084.
41. Barjaktarevic IZ and Milstone AP. Nebulized therapies in COPD: past, present, and the future. *Int J Chron Obstruct Pulmon Dis* 2020; 15: 1665–1677.
42. Dalby R, Spallek M and Voshaar T. A review of the development of respimat soft mist inhaler. *Int J Pharm* 2004; 283: 1–9.
43. Perriello EA and Sobieraj DM. The respimat soft mist inhaler, a novel inhaled drug delivery device. *Conn Med* 2016; 80: 359–364.
44. Iwanaga T, Tohda Y, Nakamura S, *et al.* The Respimat® soft mist inhaler: implications of drug delivery characteristics for patients. *Clin Drug Investig* 2019; 39: 1021–1030.
45. Xu L, Dong XW, Shen LL, *et al.* Simvastatin delivery via inhalation attenuates airway inflammation in a murine model of asthma. *Int Immunopharmacol* 2012; 12: 556–564.
46. Tulbah AS, Ong HX, Morgan L, *et al.* Dry powder formulation of simvastatin. *Expert Opin Drug Deliv* 2015; 12: 857–868.
47. Li X, Vogt FG, Hayes D Jr, *et al.* Design, characterization, and aerosol dispersion performance modeling of advanced spray-dried microparticulate/nanoparticulate mannitol powders for targeted pulmonary delivery as dry powder inhalers. *J Aerosol Med Pulm Drug Deliv* 2014; 27: 81–93.
48. Meenach SA, Vogt FG, Anderson KW, *et al.* Design, physicochemical characterization, and optimization of organic solution advanced spray-dried inhalable dipalmitoylphosphatidylcholine (DPPC) and dipalmitoylphosphatidylethanolamine poly(ethylene glycol) (DPPE-PEG) microparticles and nanoparticles for targeted respiratory nanomedicine delivery as dry powder inhalation aerosols. *Int J Nanomedicine* 2013; 8: 275–293.
49. Muralidharan P, Hayes D Jr, Black SM, *et al.* Microparticulate/nanoparticulate powders of a novel Nrf2 activator and an aerosol performance enhancer for pulmonary delivery targeting the lung Nrf2/Keap-1 pathway. *Mol Syst Des Engl* 2016; 1: 48–65.
50. Meenach SA, Anderson KW, Hilt JZ, *et al.* High-performing dry powder inhalers of paclitaxel DPPC/DPPG lung surfactant-mimic multifunctional particles in lung cancer: physicochemical characterization, in vitro aerosol dispersion, and cellular studies. *AAPS PharmSciTech* 2014; 15: 1574–1587.
51. Meenach SA, Anderson KW, Zach Hilt J, *et al.* Characterization and aerosol dispersion performance of advanced spray-dried chemotherapeutic PEGylated phospholipid particles for dry powder inhalation delivery in lung cancer. *Eur J Pharm Sci* 2013; 49: 699–711.
52. Mansour HM and Hickey AJ. Raman characterization and chemical imaging of biocolloidal self-assemblies, drug delivery systems, and pulmonary inhalation aerosols: a review. *AAPS PharmSciTech* 2007; 8: E99.
53. The United States Pharmacopoeia and The National Formulary. <601> *Aerosols, nasal sprays, metered-dose inhalers, and dry powder inhalers monograph*. USP 29-NF 24: The Official Compendia of Standards 29/24. Rockville, MD: The United States Pharmacopoeial Convention, Inc., 2006, pp. 2617–2636.
54. Meenach SA, Tsoras AN, McGarry RC, *et al.* Development of three-dimensional lung multicellular spheroids in air- and liquid-interface culture for the evaluation of anticancer therapeutics. *Int J Oncol* 2016; 48: 1701–1709.
55. Acosta MF, Muralidharan P, Meenach SA, *et al.* In vitro pulmonary cell culture in pharmaceutical inhalation aerosol delivery: 2-D, 3-D, and in situ bioimpactor models. *Curr Pharm Des* 2016; 22: 2522–2531.
56. Haghi M, Ong HX, Traini D, *et al.* Across the pulmonary epithelial barrier: integration of physicochemical properties and human cell models to study pulmonary drug formulations. *Pharmacol Ther* 2014; 144: 235–252.
57. Meenach SA, Tsoras AN, McGarry RC, *et al.* Development of three-dimensional lung multicellular spheroids in air and liquid interface culture for the evaluation of anti-cancer therapeutics *Int J Oncol* 2016; 48: 1701–1709.
58. Epithelix. *SmallAir™: a unique 3D human small airway epithelia reconstituted in vitro*. Geneva, Switzerland: Epithelix. <http://www.epithelix.com/products/smallair> (accessed September 2018).
59. Reddy VM, Meyrick B, Wong J, *et al.* In utero placement of aortopulmonary shunts. A model of postnatal pulmonary hypertension with increased pulmonary blood flow in lambs. *Circulation* 1995; 92: 606–613.
60. Johnson RC, Datar SA, Oishi PE, *et al.* Adaptive right ventricular performance in response to acutely increased afterload in a lamb model of

- congenital heart disease: evidence for enhanced Anrep effect. *Am J Physiol Heart Circ Physiol* 2014; 306: H1222–H1230.
61. Bolourchian N, Mahboobian MM and Dadashzadeh S. The effect of PEG molecular weights on dissolution behavior of simvastatin in solid dispersions. *Iran J Pharm Res* 2013; 12: 11–20.
 62. Jun SW, Kim M-S, Kim J-S, *et al.* Preparation and characterization of simvastatin/hydroxypropyl- β -cyclodextrin inclusion complex using supercritical antisolvent (SAS) process. *Eur J Pharm Biopharm* 2007; 66: 413–421.
 63. Rao M, Mandage Y, Thanki K, *et al.* Dissolution improvement of simvastatin by surface solid dispersion technology. *Dissolution Technol* 2010; 17: 27–34.
 64. Singh H, Philip B and Pathak K. Preparation, characterization and pharmacodynamic evaluation of fused dispersions of simvastatin using PEO-PPO block copolymer. *Iran J Pharm Res* 2012; 11: 433–445.
 65. Graeser KA, Strachan CJ, Patterson JE, *et al.* Physicochemical properties and stability of two differently prepared amorphous forms of simvastatin. *Cryst Growth Des* 2008; 8: 128–135.
 66. Stahlhofen W, Gebhart J and Heyder J. Experimental determination of the regional deposition of aerosol particles in the human respiratory tract. *Am Ind Hyg Assoc J* 1980; 41: 385–398a.
 67. Chew NY and Chan HK. Use of solid corrugated particles to enhance powder aerosol performance. *Pharm Res* 2001; 18: 1570–1577.
 68. Brown JS, Gordon T, Price O, *et al.* Thoracic and respirable particle definitions for human health risk assessment. *Part Fibre Toxicol* 2013; 10: 12.
 69. Crowder TM, Rosati JA, Schroeter JD, *et al.* Fundamental effects of particle morphology on lung delivery: predictions of stokes' law and the particular relevance to dry powder inhaler formulation and development. *Pharm Res* 2002; 19: 239–245.
 70. Hickey AJ, Mansour HM, Telko MJ, *et al.* Physical characterization of component particles included in dry powder inhalers. I. Strategy review and static characteristics. *J Pharm Sci* 2007; 96: 1282–1301.
 71. Tan NY and Zeitler JA. Probing phase transitions in simvastatin with terahertz time-domain spectroscopy. *Mol Pharm* 2015; 12: 810–815.
 72. Humbert M, Monti G, Brenot F, *et al.* Increased interleukin-1 and interleukin-6 serum concentrations in severe primary pulmonary hypertension. *Am J Respir Crit Care Med* 1995; 151: 1628–1631.

Visit SAGE journals online
[journals.sagepub.com/
 home/tar](http://journals.sagepub.com/home/tar)

 SAGE journals